Prospects of Aluminum Modifications as Energetic Fuels in Chemical Rocket Propulsion

Luigi T. DeLuca, Filippo Maggi, Stefano Dossi, Marco Fassina, Christian Paravan, and Andrea Sossi

Abstract The use of metals as high-energy fuels has been for long time a common approach to increase performance of chemical rocket propulsion in general. This effort was initially triggered by theoretical thermochemical considerations, but under real operating conditions, a series of collateral and unforeseen effects occurred, with both positive and negative consequences. After six decades, the use of micron-sized Al is the most common practice at industrial level for solid rocket propulsion in particular. Yet attempts are under way to mitigate some of the most deleterious effects: notably, the two-phase flow losses and slag accumulation taking place in gasdynamic nozzles. In this paper, a range of modified Al powders is discussed, going from nano-sized uncoated to coated Al particles and from chemically to mechanically activated micron-sized Al. These variants are duly characterized and comparatively tested under laboratory burning conditions. Due to page limitations, mainly the class of aluminized composite propellants (ammonium perchlorate/inert binder) and operating conditions often used in space applications are investigated. The reader is cautioned to avoid making generalizations to other formulations and conditions based on this limited dataset. Each of the tested Al variants has its own properties, and implementation in full-scale propulsive systems needs to be carefully evaluated for an overall assessment. The recommended strategy for best results is a dual mode Al mixture, synergistically exploiting each component. Other metal fuels, especially hydrides and boron compounds, are examined as well. New trends, capable of drastically changing the current situation but still in their infancy as of this writing, are briefly discussed at the end of the paper.

L.T. DeLuca (✉) • F. Maggi • S. Dossi • M. Fassina • C. Paravan • A. Sossi
Space Propulsion Laboratory (SPLab), Department of Aerospace Science and Technology, Politecnico di Milano, 20156 Milan, Italy
e-mail: luigi.deluca@polimi.it; filippo.maggi@polimi.it; stefano.dossi@polimi.it; marco.fassina@polimi.it; christian.paravan@polimi.it; andrea.sossi@mail.polimi.it

L.T. DeLuca et al. (eds.), *Chemical Rocket Propulsion*,
Springer Aerospace Technology, DOI 10.1007/978-3-319-27748-6_8

Nomenclature

a	Multiplicative factor in the Vieille steady burning rate law, (mm/s)/bar^n
actAl	Activated Al
ADN	Ammonium dinitramide
AFM	Atomic force microscopy
ALEX™	ALuminum EXploded (a trademark by APT, Tomsk, Russia)
AP	Ammonium perchlorate
APT	Advanced Powder Technologies
a_s	Mean surface particle diameter, nm
BET	Brunauer–Emmett–Teller
BPR	Ball-to-powder mass ratio
c	Specific heat, J/g K
CA	Chemical activation
C_{Al}	Active metal content, mass %
CCP	Condensed combustion products
D	particle diameter, cm
EDX	Energy dispersive X-ray analysis
EEW	Electrical explosion of wires
EM	Energetic materials
F-ALEX$_A$	ALuminum EXploded, coated by trihydroperfluoro-undecyl alcohol
F-ALEX$_E$	ALuminum EXploded, coated by ester from esterification of trihydroperfluoro-undecyl alcohol with maleic anhydride
GAP	Glycidyl azide polymer
HEDM	High-energy-density material
HMX	Cyclotetramethylenetetranitramine
HTPB	Hydroxyl-terminated polybutadiene
IARC	International Agency for Research on Cancer
ICP	Inductively coupled plasma analysis
I_s	Gravimetric specific impulse, s
I_v	Volumetric (or density) specific impulse, s·g/cm^3
k	Thermal conductivity, J/cm s K
L-ALEX™	ALuminum EXploded, coated by stearic acid
LH_2	Liquid hydrogen
LOx	Liquid oxygen
$\mathscr{M}$	Molecular mass, g/gmole
Mg_xB_y	composite metal made, in mass, by x % Mg and y % B
MM	Mechanical milling
n	Pressure exponent in the Vieille steady burning rate law
nAl	Nano-sized aluminum
NAp.	not applicable
NAv.	not available
O/F	Oxidizer-to-fuel ratio

p	Pressure, bar
P-ALEX™	ALuminum EXploded, coated by palmitic acid process control agent
PDL	Pressure deflagration limit
PTFE	Polytetrafluoroethylene
r_b	Steady burning rate, mm/s
RDX	Cyclotrimethylenetrinitramine
SEM	Scanning electron microscopy
SPLab	Space propulsion laboratory
SRB	Solid rocket booster
SRM	Solid rocket motor
S_{sp}	Specific surface area, m^2/g
TEM	Transmission electron microscopy
TG	Thermogravimetry
T_{melt}	melting temperature, K
T_{vap}	vaporization/decomposition temperature, K
VF-ALEX	ALuminum EXploded, coated by Fluorel™ FC-2175 (copolymer of vinylidene fluoride and hexafluoropropylene made by 3M) and ester
XRD	X-ray diffraction analysis
Δh_f^0	Standard heat of formation, kJ/mole (see Table 1)
Δh_{melt}	melting enthalpy, kJ/mole (see Table 1)
Δh_r	reaction enthalpy, kJ/g or kJ/cm^3 (see Table 1)
Δh_{vap}	vaporization/decomposition enthalpy, kJ/mole (see Table 1)
ΔV	Vehicle velocity increment, m/s
μAl	Micron-sized aluminum
ρ	Density, g/cm^3

1 Background

Although the first suggestion by Tsander to use aluminum as high-energy fuel dates back to 1909, testing of metals, or metallic compounds, started only after the Parson discovery of castable composite propellants in 1942. However, a lot of attempts and efforts were needed before Henderson and Rumble succeeded in adding Al powder, thus significantly increasing the propellant specific impulse in 1955. For historical details, see chapter "Highlights of Solid Rocket Propulsion History" in this book.

As a matter of fact, metals in general burn with marked difficulties due to resistance to ignition, uncertain dynamics of the combustion process in both homogeneous and heterogeneous phase, and unlikely completion of the underlying oxidation reactions. Even larger difficulties are faced by the resulting two-phase mixtures during expansion in the gasdynamic nozzle. The main reason for these difficulties lies in the fact that the condensed-phase reaction products result in two-phase flows where physical aspects dominate over chemistry in combustion chambers and over gasdynamics in nozzles. The associated performance losses could totally be eliminated by employing substances based on F_2 instead of O_2

as the oxidizer, thus yielding volatile rather than condensed combustion products. Unfortunately, both F_2 and its combustion products are extremely toxic and therefore will likely be utilized only in deep space missions.

During combustion, metallic powders release considerable energy due to their high enthalpy of combustion, thus increasing the adiabatic flame temperature and subsequently the propellant gravimetric specific impulse (I_s) in spite of the simultaneous increase of the average molar mass of the combustion products. Metals also increase the propellant density and subsequently the propellant volumetric specific impulse (I_v). Both effects are consistent with primary requirements for space propulsion missions [1, 2]. An unforeseen but very welcome additional effect is the consequent resistance to high-frequency combustion instabilities revealed by metalized formulations. However, concomitant drawbacks were soon discovered: the remarkable increase of adiabatic flame temperature also implies a dangerous increase of thermal fluxes to the motor walls and subsequently an increase of the motor inert mass fraction needed to accommodate more ablative material. A range of detrimental effects takes place in the gasdynamic nozzle, especially in the throat area region, all implying I_s losses due to two-phase flow with subsequent thermal and kinetic nonequilibrium, slag accumulation, nozzle submergence, and nozzle erosion. Also, the emission of a plume consisting of intense primary white smoke of alumina (for Al burning) and electrically charged particles hindering electromagnetic communications is not appreciated by both military bodies and green organizations defending the environment.

Aluminum is one of the most commonly used metal fuels because of its high oxidation enthalpy under a variety of oxidizing atmospheres, high density, low price, good availability, and low oxygen demand. Micron-sized aluminum (μAl) powders have been used for decades in solid propellants to increase the formulation specific impulse and the resistance to high-frequency acoustic instabilities. However, the clustering/aggregation effects of μAl particles, occurring under certain conditions prior to their ignition, favors the deleterious agglomeration phenomena due to inflammation and coalescence by melting. This leads to specific impulse losses due to incomplete metal combustion and two-phase flow effects. In hybrid rocket fuels, μAl has been used, without success, to augment the radiative heat feedback from the flame zone to the gasifying surface, the aim being to increase the regression rate, which is currently one of the limiting factors of these propulsive systems.

Combustion of Al in propulsion applications turns out to be an extremely complex and multifaceted process. Even though most of the Al particles burn as a single particle, either on the burning surface or far from it, a significant fraction of the total Al mass burns as clusters of particles. This is due to a highly intricate mechanism of cohesion, exudation, aggregation, and agglomeration that likely starts in the subsurface region and continues in the convective two-phase flow issued from the surface until all reactions stop at a relatively large distance from the surface. Rarely are these processes finished at the surface. At any rate, the simultaneous occurrence of homogeneous combustion (yielding fine products of reaction) and heterogeneous combustion (yielding coarse products of reaction) eventually gives rise to a bimodal product distribution. While the homogeneous combustion in the

gas phase is believed to be well understood, its heterogeneous counterpart is only poorly known.

An alternative approach of strong interest is to use hydrides instead of the corresponding metals [3]. In this respect, AlH_3 and BeH_2 come out especially attractive and promise significant increase of the ideal gravimetric specific impulse for solid and hybrid propellant rockets. Hybrid rocket engines based on BeH_2 can achieve, at least theoretically, the maximum performance in the field of chemical propulsion, much above that of the current cryogenic couple LH_2/LOx. However, beryllium is not allowed due to its toxicity, and hydrides are in general difficult to synthesize and typically manifest problems of chemical instability. That is, they spontaneously release H_2 after some more or less extended lapse of time.

In general, in a composite formulation, hydrogen release from hydrides is a fast process with respect to the competing binder decomposition and thus acts to sustain and intensify the surrounding flame with prompt and fast hydrogen diffusion. However, metals and metal hydrides are different energetic ingredients and follow different mechanisms during the overall combustion process, even with respect to the basic metal component. In particular, rapid dehydrogenation of metal hydride particles during the combustion process leaves behind a porous metal matrix due to the cavities formed by the gasified hydrogen. The final result is a metallic structure much more reactive than the corresponding solid metal, even if shaped as a micron-sized particle.

Conventional μAl powders have been ineffective in enhancing either the burning rate of solid propellants or regression rate of solid fuels in hybrid propellants. Thus, propellant formulators have directed their attention to suitable variants of the μAl powders such as nano-sized aluminum (nAl) powders, chemically activated μAl powders, mechanically activated μAl powders, boron compounds, and so on with the intent of mitigating the ballistic drawbacks of the conventional μAl powders [4]. This paper will discuss the prospective of μAl powder variants as energetic fuels under laboratory conditions. Agglomeration phenomena are observed near/at the burning surface (incipient agglomeration) and no attempt is made to discuss combustion modeling. The reader is expected to be familiar with the open literature available in this area. Due to page limitations, priority will be given to solid rocket propulsion, focusing on formulations and operating conditions commonly used in space launchers. A companion paper devoted to hybrid rocket propulsion is authored by Karabeyoglu in this volume [5]. A variety of potentially useful additives for improving the regression rate or system performance of hybrid rocket engines was tested and reported in a referenced paper [6].

2 Thermochemical Properties

The use of metal powders in hybrid and solid propulsion pursues different targets. Both gravimetric and volumetric specific impulses can be incremented in solid propellants, depending on the specific additive. The former takes advantage of

combustion enthalpy, while density increment favors the latter one. For hybrid rocket propellants, the addition of metals depresses the gravimetric specific impulse I_s due to the increment of the molar mass of the combustion products. However, density increment represents an important contribution to obtain a higher mass burning rate.

2.1 Metal Fuels

In the open literature Al, Be, B, Li, Mg, Na, Zr, Fe, Cr, and other metals are commonly considered for space applications. The scope of their use can range from increasing enthalpy release, improving either specific impulses or density, or acting as a combustion catalyst. The current industrial state of the art considers the use of micrometric powders. In most cases, there are nanometric alternatives, but several issues related to safety, processing, handling, storing, dispersion, aging, and cost are introduced [7].

Out of this group, there is interest in using Al, B, Mg, and Zr as metal fuels. Beryllium and its derivatives are considered carcinogens by IARC, discouraging their application [8].

Aluminum is one of the most common components in space propulsion. It is an amphoteric metal whose density is 2.70 g/cm^3. The oxidation of Al to the aluminum (III) oxide (alumina, α-Al_2O_3) generates a heat of reaction of 31.07 kJ/g (83.89 kJ/cm^3) [9]. It features a low toxicity and, as micrometric particles, is relatively safe and easy to compound. Aluminum's positive contribution to ideal performance is calculated for solid propellants, both for its density and for its enthalpy release. The combustion of this material generates condensed products which can be liquid or solid particles, depending on local temperature.

Magnesium is a metal which is fairly easy to ignite and oxidize and has a density of 1.74 g/cm^3. It is considered a low-performance alternative to Al, with lower gravimetric and volumetric heat of reaction, 24.7 kJ/g and 43.0 kJ/cm^3, respectively [10]. Reactivity of Mg is exploited to promote the reaction of other metals which are more reluctant to ignite, such as boron.

Boron is a metalloid with density of 2.34 g/cm^3. Its oxidation to solid boron (III) oxide B_2O_3 generates a theoretically high value of both gravimetric and volumetric heat of reaction (58.86 kJ/g and 137.73 kJ/cm^3, respectively), making it a good candidate for high energy-density applications [9]. The B_2O_3 has a boiling point of about 2300 K, so it appears that the full exploitation of B combustion energy release can be obtained only if condensation of the oxide is ensured in the propulsion system [11]. On the other hand, oxide vaporization contributes to the reduction of condensed combustion products and of related specific impulse losses. In actual use, poor particle ignition results in a low combustion efficiency. Recent developments in magnesium–boron alloys enabled rapid particle ignition and efficient combustion [12].

Zirconium has a density of 6.52 g/cm^3 and has mostly been used to increment the density of the propellant. Oxidation to zirconium (IV) oxide (zirconia, ZrO_2) does not provide an attractive gravimetric heat of combustion, which is 12.03 kJ/g. But because of the high density, the volumetric heat release is 78.43 kJ/cm^3 [9].

2.2 Ideal Computed Performance

The performance of solid rocket propellant and hybrid fuel alternatives can be predicted and compared via thermochemical calculations based on the characteristics of the ingredients in the initial composition and their total enthalpy (formation and sensible). Information on combustion products can be obtained, as well. In these calculation techniques, the physical organization of the mixture (e.g., in bricks, micrometric particles, or nanopowders) has no meaning, unless connected to a significant energetic contribution. For example, in the case of nanometric particles, a surface energy may be associated to the size, due to the increasing ratio between superficial and bulk atoms, but this effect is negligible for the range of interest (namely, 100 nm or above) [13, 14]. At the same time, the difference between nominal and real powder composition has to be considered, if passivation layers or surface treatments measurably affect the active metal content.

The following performance data are computed assuming chemical equilibrium in the combustion chamber and, locally, in the nozzle. Reference combustion chamber pressure is 70 bar, nozzle area ratio is 40, and vacuum conditions are assumed. Solid propellant formulations composed of hydroxyl-terminated polybutadiene binder (HTPB, $C_{7.075}\ H_{10.65}\ O_{0.223}\ N_{0.063}$, $\Delta h_f^0 = -58$ kJ/mole) and ammonium perchlorate (AP, NH_4ClO_4, $\Delta h_f^0 = -295.8$ kJ/mole) as oxidizer [15] are compared below. Hybrid rocket performance is evaluated for HTPB binder and liquid oxygen (LOx, $O_{2(l)}$, $\Delta h_f^0 = -13$ kJ/mole), at the boiling point of 90 K [10].

Figure 1 reports volumetric and gravimetric specific impulse for solid propellants having a fixed AP/metal/HTPB formulation of 68/18/14 mass fraction. Figure 2 reports the same data for HTPB/metal hybrid rocket fuels with 90/10 mass fraction. For solid propellants, the aluminum is the metal featuring the highest I_s and I_v. Zirconium has the lowest I_s, but it ranks second for I_v, due to metal density. The other fuels have lower I_v and intermediate I_s. The reader should note that the proposed formulations are not optimal because the stoichiometric oxidizer requirement of the various metals is ignored. AP/metal/HTPB compositions are compared on the basis of equal mass of added metal.

In hybrid rockets, all metals lower the maximum I_s capability, but performance does not change dramatically, with the exception of an oxidizer/fuel shift towards lower value of curve peak. The use of Al or B gives better results than other proposed candidates. The higher density of the metalized polymer fuel improves I_v. The use of Al, B, and Zr enables higher I_v, if compared to Mg and pure HTPB.

The relevant properties of the selected metals (Al, B, Mg, Zr) and of their most common oxides are summarized in Table 1. The volumetric heat release is maximum for B, followed by Al and Zr; while the gravimetric heat release is maximum for B,

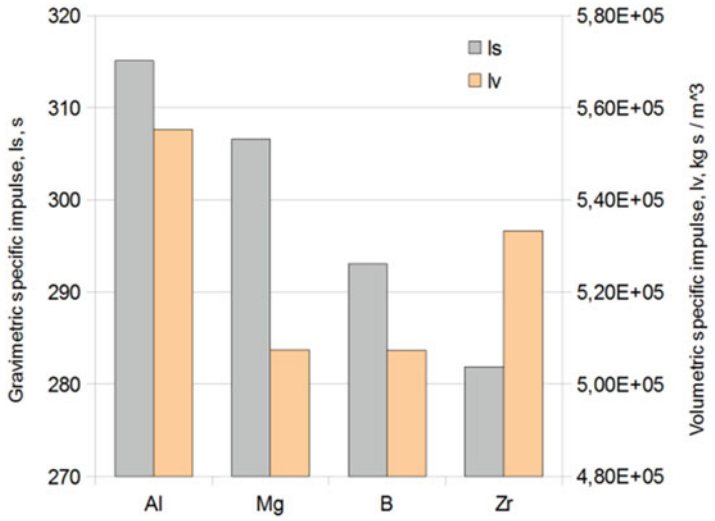

Fig. 1 Solid propellant performance parameters for fixed composition of 68 mass % AP, 14 mass % HTPB, and 18 mass % of metal fuel

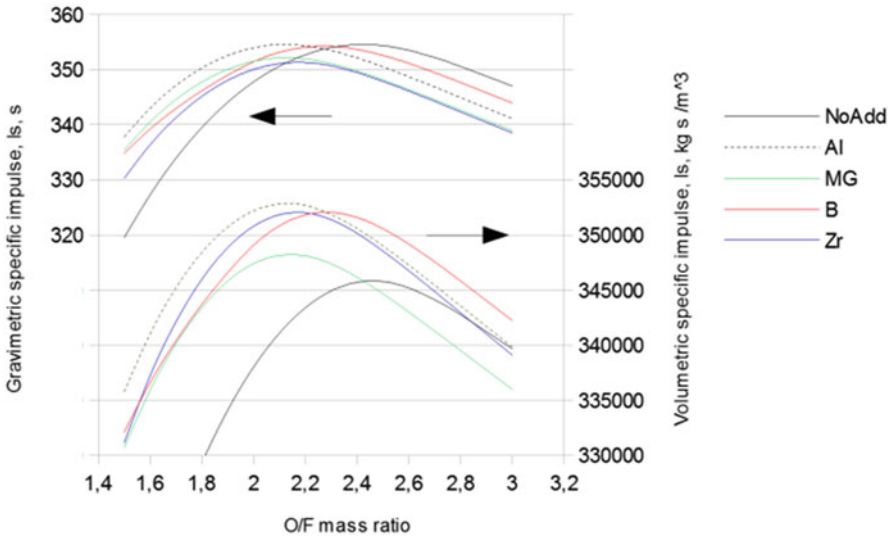

Fig. 2 Hybrid rocket performance parameters for 90 mass % HTPB and 10 mass % metal fuel burning in LO_x

Table 1 Properties of currently used metallic fuels and their most common oxides

Metals and most common oxides	ρ, g/cm^3	$\mathcal{M}$, g/mole	$\Delta h_f{}^0$, kJ/mole	T_{melt}, K	Δh_{melt}, kJ/mole	T_{vap}, K	$\Delta h_{vap}{}^a$, kJ/mole	$\Delta h_r{}^c$, kJ/g	$\Delta h_r{}^c$, kJ/cm^3
Al	2.70	27.0	0	933 [16]	10.7 [16]	2792 [16]	294 [16]	31.07	83.89
Al_2O_3	3.99	102.0	−2550	2327 [16]	111.1 [16]	3253 [16]	109 [18]	NAp.	NAp.
B	2.34	10.8	0	2348 [16]	50.2 [16]	4273 [16]	480 [16]	58.86	137.73
B_2O_3	2.55	69.6	−1272	723 [16]	24.6 [16]	2133 [17]	360 [17]	NAp.	NAp.
Mg	1.74	24.3	0	923 [16]	8.5 [16]	1380 [18]	136 [18]	24.70	43.00
MgO	3.60	40.3	−601	3098 [16]	77[d] [16]	3430[b] [17]	670 [17]	NAp.	NAp.
Zr	6.52	91.2	0	2125 [19]	21.0 [19]	3850 [19]	573 [19]	12.03	78.43
ZrO_2	5.68	123.2	−1097	2951 [19]	87.0 [19]	4573 [19]	624 [19]	NAp.	NAp.

[a] At boiling point
[b] Metal oxides are subject to vaporization-decomposition phenomena [17]
[c] O_2 reaction
[d] Unknown with enough accuracy

followed by Al and Mg. The metal melting temperature is much less than that of the corresponding oxide for Al and Mg, while the opposite is true for B. The peculiar properties of B hamper its efficient combustion and nozzle expansion. The interest for Zr in propulsion applications is explained by its large value of density, making possible remarkable ΔV increments of the vehicle velocity [1].

3 nAl Powders

The best-known variant of the conventional μAl powders is the nAl powders first tested by Gen et al. in 1978 [20]. In a flow of oxygen-containing gas, they burned nAl produced by vaporization and consequent condensation of the metal vapors in Argon (as invented by Gen et al. in 1959 [21]). A significant decrease of the CCP (condensed combustion product) size was observed. While the initial expectation of an increased internal energy for nAl powders was disproved (for the typical size of interest in propulsion), it is true that the large specific surface area of nAl makes oxidation rates much higher favoring the heterogeneous metal attack compared to the homogeneous one, because of greatly reduced diffusion lengths.

3.1 Production and Characterization

The knowledge of thermophysical properties of energetic additives prior to their employment in energetic formulations is needed to make reliable assessments about their reactivity and interaction with the external environment. The following paragraphs contain the results of experimental thermophysical investigations carried out on several nAl powders, passivated and coated with various chemical species. For details about tools and diagnostics, see [22].

Today an efficient method for obtaining submicron-sized metal powders is the electrical explosion of wires (EEW) technique, in which electrical energy is almost totally consumed for the metal wire gasification [23]. In the case of Al, the metal powders must be passivated by an inert coating immediately after production, due to their pyrophoric behavior. The passivation process can be done by a slow stream of dry gases (Ar + 0.1 % air) or by means of different chemical substances, other than air. The commercial name for nAl powders passivated by aluminum oxide is ALEX™ [24]. The purpose of coating the metal powders with chemicals is to improve their dispersion inside the matrix, mechanical properties and combustion processes of the final formulation. Specific coatings can be chosen to protect the particle surface from the oxidation by air or atmospheric moisture [25].

In this work, two batches of ALEX™ with nominal size of 50 and 100 nm are considered. They were manufactured by a coating process at lab scale [26] as:

- Stearic and palmitic acid (L-ALEX, P-ALEX)
- Trihydroperfluoro-undecyl alcohol (F-ALEX$_A$)

- Ester from esterification of trihydroperfluoro-undecyl alcohol with maleic anhydride (F-ALEX$_E$)
- Fluorel™ FC-2175 (copolymer of vinylidene fluoride and hexafluoropropylene made by 3M) and ester (VF-ALEX)

Such powders were characterized and tested as energetic additives to evaluate the regression rate enhancement with respect to pure HTPB solid fuel for hybrid rockets [27]. Samples of 50 and 100 nm stearic acid-passivated nAl powders are considered as well, in order to assess the differences between industrial-scale passivated powders and lab-scale powders which are coated after passivation.

3.2 Electron Microscopy Analyses

Uncoated powders display spherical shape of particles, as well as fatty acid-coated nAl (see Fig. 3). The presence of flake-shaped structures in uncoated powders is indicative of possible clustering of particles due to the explosion process and cold cohesive forces between granules or cold sintering processes due to the high specific surface area. Signs of the coating manufacturing process are visible in Fig. 4, in which the incomplete solution of fluoropolymer or its return to the solid state after solvent removal is recognizable.

The different image formation mechanism of TEM with respect to SEM provides different information about coating thickness and nAl particle aggregation to be gathered. It is possible to recognize the thin, brighter layer surrounding the metal core in the case of air-passivated powders (ALEX™ samples). Moreover, the formation of a double shell structure with the coating surrounding the air-passivated particle is clearly visible; see Fig. 5.

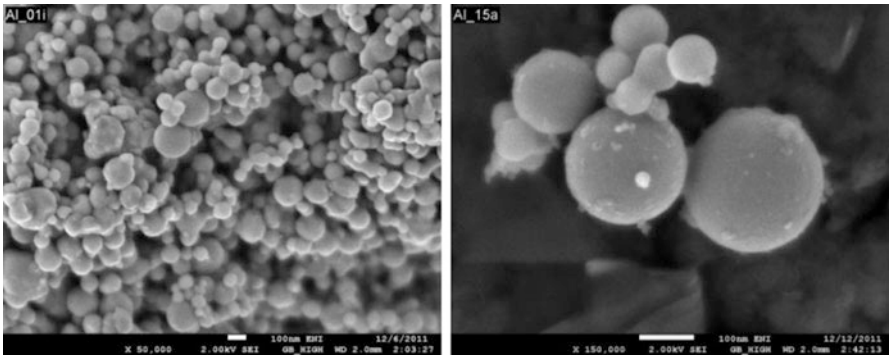

Fig. 3 SEM images of 100 nm ALEX™ (*left*) and 50 nm palmitic acid-coated P-ALEX (*right*)

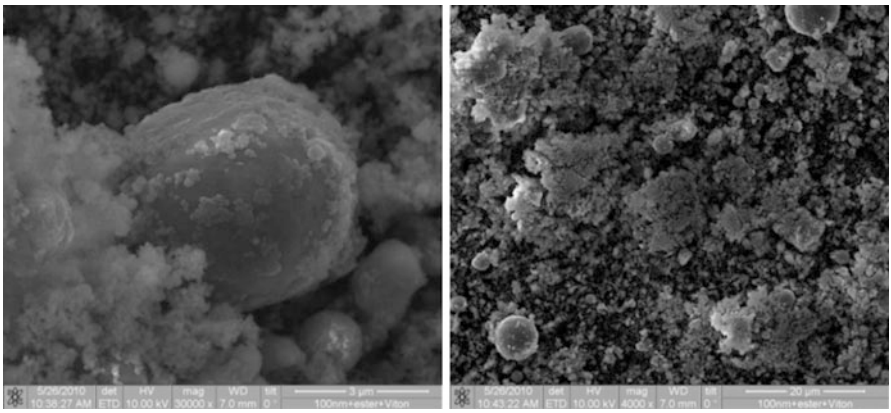

Fig. 4 SEM images of 100 nm Fluorel™ and ester-coated VF-ALEX

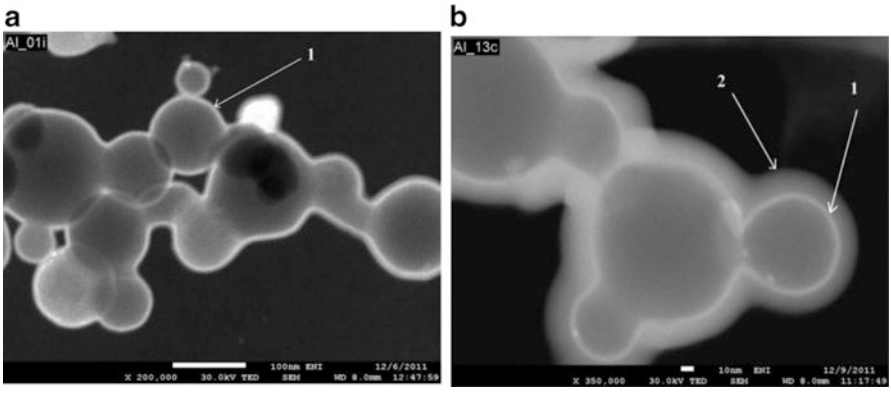

Fig. 5 TEM images of nAl [*1* oxide layer; *2* coating layer]: (**a**) 100 nm uncoated ALEX™; (**b**) 50 nm Fluorel™ and ester-coated VF-ALEX

3.3 Physical Analyses

The specific surface area S_{sp} of the nAl powders was evaluated by a BET approach. The active metal content C_{Al} was determined through a volumetric method [28]. Assuming spherical and nonporous particles of density ρ_{Al}, the mean surface particle diameter a_s can be calculated from S_{sp} (Tables 2 and 3), as

$$a_s = \frac{6}{S_{sp}\rho_{Al}} \tag{1}$$

As expected, the BET S_{sp} of 50 nm ALEX™ is greater than that of 100 nm ALEX™. The lowest S_{sp} belongs to Fluorel™ and ester-coated powders, which

Table 2 Physical parameters of 50 nm nAl powders

Powder	BET S_{sp}, m^2/g	a_s, nm	C_{Al}, mass %	ρ_p, g/cm^3
ALEX™	15.7	142	90	2.503
L-ALEX[a]	11.3	197	89	2.329
P-ALEX	13.9	160	71	2.491
VF-ALEX	10.9	204	78	2.559

[a]Stearic acid-passivated

Table 3 Physical parameters of 100 nm nAl powders

Powder	BET S_{sp}, m^2/g	a_s, nm	C_{Al}, mass %	ρ_p, g/cm^3
ALEX™	11.8	188	89	2.522
L-ALEX	9.1	244	70	2.474
P-ALEX	NAv.	NAv.	79	2.448
F-ALEX™	11.3	197	88	2.586
VF-ALEX	6.9	322	78	2.518

is clear evidence of effective coating deposition (and possible effects of particle clustering induced by the coating process itself). An increase of the average particle size related to the coating thickness diminishes the powder specific surface.

The remarkable difference in active Al content, between uncoated ALEX™, stearic acid-passivated L-ALEX, and coated variants, is explained by the presence of a double shell structure for the latter, consisting of a passivating plus a coating layer.

A large amount of data was also provided by DSC and TG traces. A first strong oxidation peak of aluminum and a second less intense oxidation phase above the melting point testify the periodic cracking of the oxide shell surrounding the metal core and the separate oxidation of different particle fractions. These and other data clarify important details about the powder reactivity, as discussed in [22]. However, heating rates are lower by orders of magnitude with respect to those typical of rocket operating conditions. Thus, how to efficiently apply such data to propulsive systems remains a matter of study.

3.4 Suspension Rheology and nAl Dispersion

Heterogeneous solid propellants and solid fuels for hybrid propulsion are formulations containing disperse systems embedded in a binder matrix. The binder is usually an elastomer, typically a polyurethane [29]. Different materials can be considered for this task based on specific requirements such as chemical compatibility or ballistic performance [30]. A commonly used binder in propulsion applications is HTPB. During the propellant/fuel preparation, and after its curing, the rheological behavior of the binder is influenced by the filler addition.

The reduced size and the increased S_{sp} value of nano-sized materials promote their clustering or cold cohesion effects. Due to this effect, the processing of nanomaterial-loaded formulations requires dedicated powder dispersion procedures. The most explored dispersion strategies are based on ultrasonication of particle suspension and use of dispersive agents. For details, see [31, 32] and, in this book, [33].

3.5 nAl Burning in Solid Propellants

Aluminized composite solid rocket propellants loaded with μAl have been studied for decades under a variety of operating conditions, and their ballistics is quite well known; see, for example, [34–36]. Inert binder formulations containing nAl particles, show faster steady burning rates compared with the corresponding propellants containing μAl particles. Nano-sized Al particles manifest a strong reactivity mainly due to their increased specific surface area, notwithstanding the simultaneous decrease of active Al content. Oxidation of nAl is completed very close to/above the burning surface following a form of prompt partial oxidation at/below the burning surface.

The results obtained in previous experimental studies conducted at SPLab can be summarized by the plot in Fig. 6; for details, see [22, 37–43]. Under the common laboratory operating conditions explored for AP/HTPB-based formulations up to

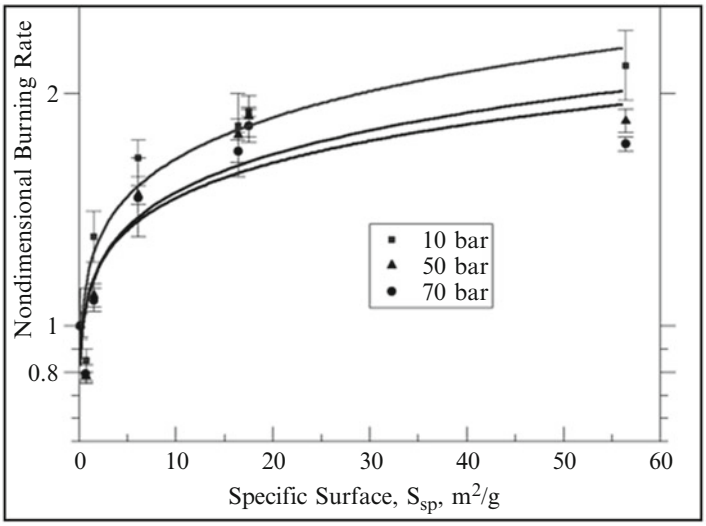

Fig. 6 Normalized steady burning rate vs. BET-specific surface, for solid propellants loaded with nAl powders, showing different sensitivity over the explored S_{sp} range [43]

70 bar, steady burning rates measured for propellants loaded with a variety of Al powders show different sensitivity over the tested S_{sp} range. The observed values are not significantly affected by particles in the micrometric range (say, $S_{sp} \leq 2$ m^2/g), but are strongly increased as the particle size is reduced over the explored nanometric range. The strongest sensitivity in increasing the propellant steady burning rate is noticed for nAl in the range 0.1–0.2 μm (i.e., with S_{sp} in the range 5–20 m^2/g). For the very smallest particles, the appreciable decrease of active metal content hinders a further increase of the propellant steady burning rate in spite of the very fast particle oxidation rate. The maximum propellant steady burning rate increase is by a factor of 2 for S_{sp} approaching 60 m^2/g over the pressure range 10–70 bar. Within the limits of the reported strand burner experiments, pressure exponents in general show only minor changes.

Also for ignition delay, an appreciable decrease is found for solid propellants containing nAl particles in the range 0.1–0.2 μm compared to μAl, while a slight increase was observed for μAl compared to the nonaluminized formulations, due to the increased thermal responsivity $(k \cdot \rho \cdot c)^{1/2}$ of the propellant condensed phase.

3.6 Agglomeration Process

Al particles undergo several events during combustion process. A particular propellant microstructure feature entails the formation of fuel-rich regions, where binder, Al particles, and fine particles of AP are present in high concentrations, confined by coarse AP crystals. These regions, the so-called pockets discussed by Zarko et al. [44] and Cohen [45] or skeleton layer extensively discussed by Babuk et al. in [46–49] and [50] in this book, are where the principal processes connected to Al transformation take place during combustion. An alternative approach has also been developed based on a statistical interpretation of the pockets present in the propellant microstructure [51, 52]; a recent study is due to Maggi et al. [53].

Figure 7 illustrates how Al particles are dispersed into solid propellant and shows μAl more dispersed with respect to nAl. Two-phase flow losses depend on the presence of condensed products during combustion, mainly Al and Al_2O_3. The sequence of events related to combustion of Al particles is rather complex. The Al powder is first exposed on the burning surface as solid particles coated by molten/decomposed binder and roughly keeping their initial geometry, below the Al melting temperature of 933 K. Then, most of the exposed Al particles burn as single particles, either on the burning surface or far from it, while a significant fraction of them (about one third in the case of Ariane-5 SRB) burns as clusters of particles forming spherical agglomerates of liquid Al and Al_2O_3 with a solid lobe of Al_2O_3.

The aggregation/agglomeration phenomena observed near the burning surface appear quite different for nAl formulations compared with μAl formulations. A comparison between the different transformations of μAl and nAl powders during the combustion process is shown in Fig. 8 [38, 40]. Propellants loaded with nAl form aggregates (flakes) with coralline structures and of limited size on the

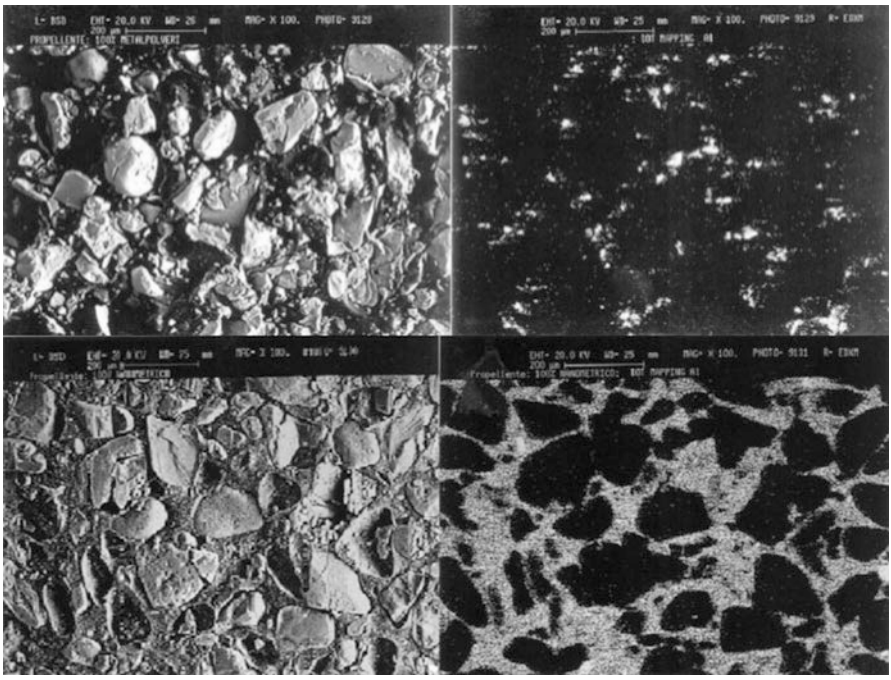

Fig. 7 SEM (*left*) and EDX (*right*) images of solid propellant 68 % AP + 17 % HTPB + 15 % Al. *Top images* show surface dispersion of μAl particles (flakes of 50 μm characteristic size), while *bottom images* show surface dispersion of nAl (uncoated ALEX) [43]

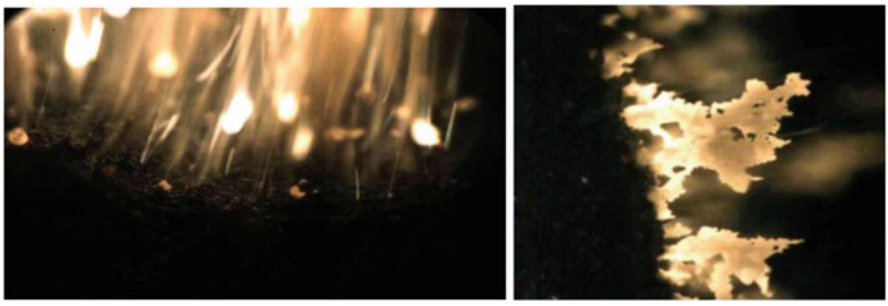

Fig. 8 Agglomeration process for μAl (on the *left*) and nAl (on the *right*) [38]

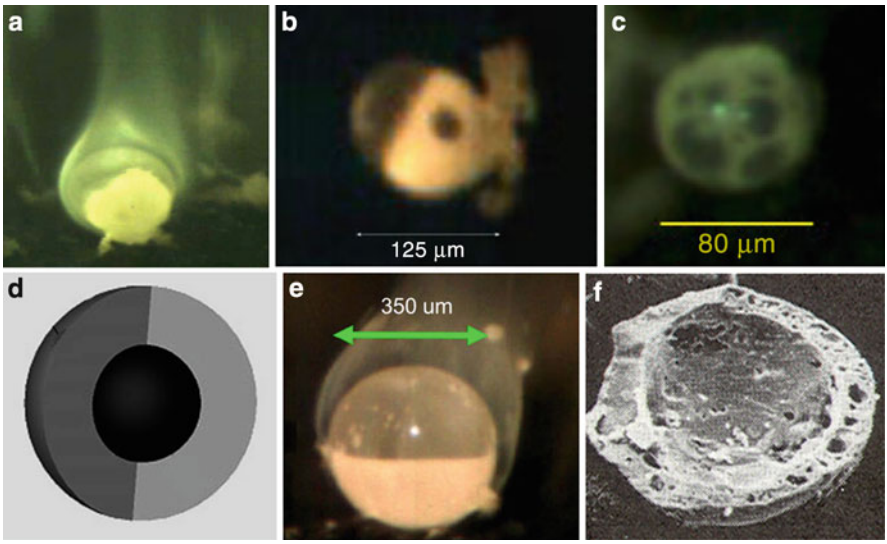

Fig. 9 Morphology of agglomeration: (**a**) burning oxide cap agglomerate from AP/µAl propellants [38], (**b**, **c**) burning matrix agglomerate [38], (**d**) sketch of metal core coated by an oxide layer [48], (**e**) burning metal cap agglomerate from AN/µAl propellants [38], (**f**) residual hollow shell [54]

burning surface, whereas µAl generates droplets that may reach up to several hundred micrometers near (at or above) the surface. For uncoated nAl burning under subatmospheric pressure, about 80 % γ-Al_2O_3 and δ*-Al_2O_3 were recovered, while up to 10 % was unburned Al and the remaining CCP consisted of intermediate products, such as Al_2OC and Al_4C_3. A comparative survey of possible agglomerates or CCP shapes is shown in Fig. 9: the oxide cap agglomerate is typical of AP/µAl (image a), the matrix agglomerate is typical of AP/AlH_3 (images b and c), the oxide layer coating the metal core is typical of AP/nAl (image d), and the hollow metal cap agglomerate is typical of AN/µAl (images e-f). Systematic analyses on agglomerate size have been carried out by Babuk [46–50], while fundamentals of particle size analysis in solid rocket propulsion were treated by Kraeutle [54]. Further effects are described in this book by Weiser et al. [55].

3.7 Nomenclature for Cohesion, Aggregation, and Agglomeration

To distinguish the different ways that the complex phenomena of; particle clustering manifest themselves, the following nomenclature is used here [22, 42, 43]. The word agglomeration is reserved to the formation of the spherical drops of liquid

metal and oxide in combustion, while the word aggregation is reserved to the formation of the partially oxidized flakes of irregular shape seen at or near the burning surface (an intermediate step between the initial form of the metal and the possible final spherical agglomerates). Agglomerates always imply a loss of the initial particle individuality; aggregates are agglomeration precursors and may keep some semblance of the initial particle individuality. As defined, both agglomeration and aggregation are processes typically occurring at high temperatures during Al burning. In addition, it is convenient to reserve the word cohesion for describing "a portion of a substance cleaving together in a thick nondescript mass" (Webster's Dictionary).

3.8 Comparative Combustion Testing of μAl vs. nAl Formulations

The superior ballistic properties of nAl in terms of steady burning rate, as just summarized, are well known in the open literature. This effect is typically ascribed to the more intense heat release rate near the burning surface compared to that occurring in the corresponding μAl formulations. The minute local space and time scale, however, make very difficult to directly map the heat release rate near the burning surface. But an indirect proof can be obtained by comparing the burning response of solid propellants, featuring the same composition but loaded with different Al particles size (μAl was replaced by nAl), under specific operating conditions:

- Dynamic extinction by fast depressurization
- Static extinction by pressure deflagration limit
- Steady burning near pressure deflagration limit
- Laser radiation ignition

The common formulation of the tested aluminized propellant was AP 68 % + HTPB 17 % + Al 15 %. Two variants were manufactured differing only by the type of Al powder incorporated: 50 μm nominal size μAl (flakes SPLab-06) and 0.150 μm nominal size nAl (air passivated, uncoated SPLab-01a). The data previously collected with an AP 80 % + HTPB 20 % nonmetallized propellant were used as reference. The measured steady-state burning rates for the nAl propellant are higher than for the μAl propellant. For the specific composition tested in this experimental campaign, Vieille's law exponent decreases from 0.56 for the μAl propellant to 0.42 for the nAl propellant. On the contrary, adding μAl to a nonmetallized propellant does not significantly modify the ballistic properties of the propellant; for details see [22].

3.9 Fast Depressurization

The two selected solid propellants were then tested under transient combustion to assess their intrinsic resistance to strong but well-controlled dynamic disturbances. The go/no-go boundary between (continued) combustion and extinction was obtained in the same experimental apparatus. The go/no-go data were plotted in terms of initial depressurization rate vs. initial pressure. A straight line was found to separate the extinction region from the burning region.

If the combustion of nAl formulations truly involves a more vigorous energetic coupling at the burning surface in terms of increased heat feedback, this effect should clearly manifest itself in the experimental results of dynamic extinction boundary by fast depressurization. In fact, testing revealed a great increase of the depressurization rate needed to extinguish the nAl propellant. In the experimental apparatus used in these tests, extinction of the nAl propellant required an exhaust orifice area about four times the one required by the μAl propellant.

In Fig. 10 the dynamic extinction boundaries of the different test propellants in terms of initial depressurization rate vs. initial pressure are reported. Even in this case, the behavior of the μAl propellant and that of the reference non-metallized propellant are comparable, with differences of the order at most of 20 %. However, these differences are negligible if compared to the depressurization rate values associated with the nAl propellant. As a matter of fact, a 400 % increase of the depressurization rate is needed for the nAl composition to achieve extinction.

In contemplating the results presented above, one should also take into account the decrease of condensed-phase characteristic time for the conductive thermal wave. Assuming a constant thermal diffusivity of the condensed phase, the steady burning rate increase leads to a thermal wave characteristic time ≈75 % lower.

An additional effect is illustrated in Fig. 11, showing the Al particle distribution on the propellant surface before combustion and after quenching by fast depressurization. This visualization was obtained by superimposing an EDX microanalysis map on the corresponding SEM image. Because of the molten layer of binder during the combustion process, compared to μAl the nAl particles can disperse on the surface more uniformly and compatibly with the AP grain size distribution.

3.10 Pressure Deflagration Limit (PDL)

Pressure deflagration limit (PDL) phenomena are of interest for low-pressure operations in general, ignition, safe storage and transport, controlled extinction phenomena, etc. For a finite sample geometry, burning is no longer self-sustained for pressures below PDL. For a given formulation, the intrinsic value of PDL actually corresponds to a sample of infinite geometry, i.e., unaffected by border effects. In practical terms, the importance of the border effects is assessed by the shape

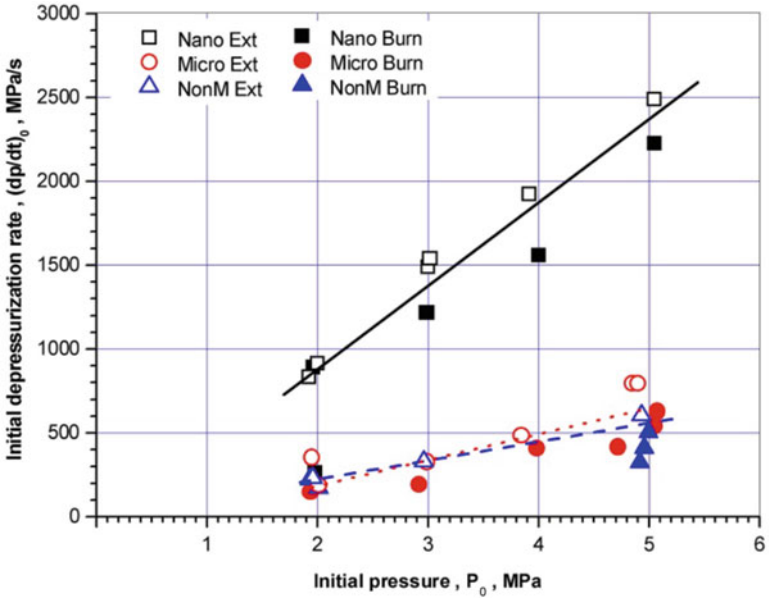

Fig. 10 Dynamic extinction boundaries by fast depressurization of three formulations [56]

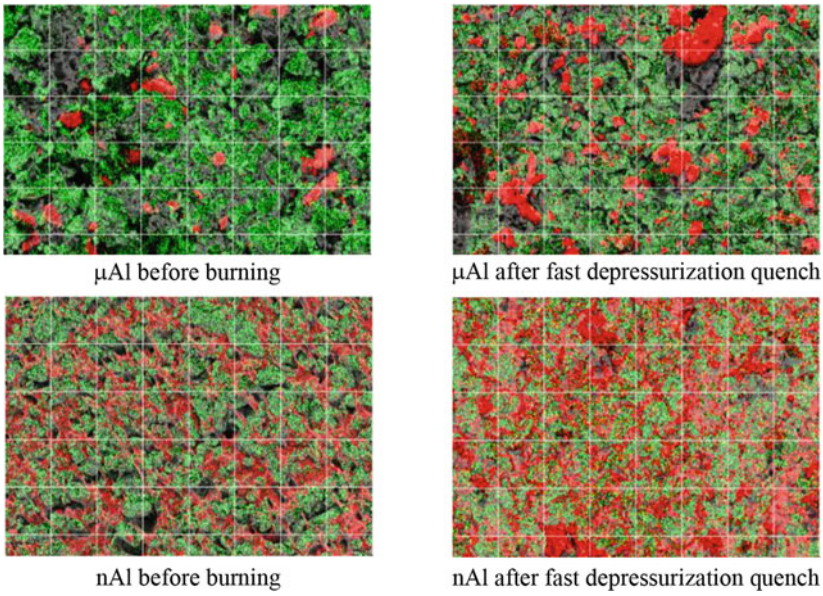

Fig. 11 Morphology and composition maps of unburned (*left*) and quenched (*right*) surfaces of μAl (*top*) and nAl (*bottom*) propellants (Al in *red* and Cl in *green*) [56]

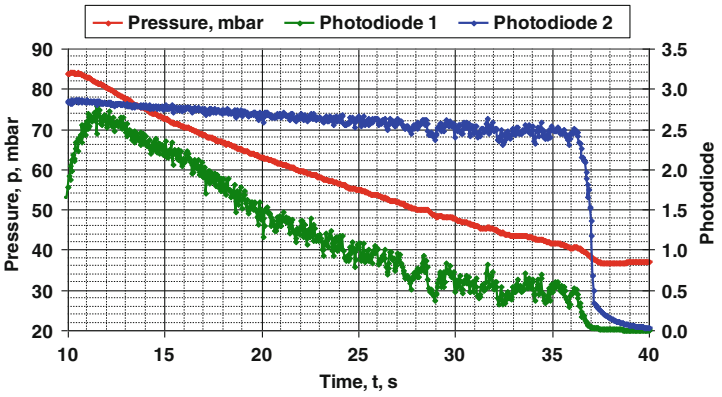

Fig. 12 Photodiodes and pressure transducer signals during PDL testing [56]

factor, defined as the characteristic (area/perimeter) sample cross section ratio. The experimental results obtained at SPLab point out a lower PDL, and thus stronger resistance to static extinction, for propellants using nAl instead of μAl.

Tests were performed in an experimental rig purposely designed for this task; for details see [22]. Propellant samples were ignited at a pressure slightly higher than the expected PDL; the pressure was then smoothly reduced till complete extinction was reached. By direct observation of the signals of the photodiode and pressure transducer (Fig. 12), a peculiar trend can be recognized. The central part of the combustion is characterized by decreasing pressure, while the photodiodes show a reduction of frequency of the oscillating combustion and an increase in amplitude; when the flame extinction is reached, the signal from the photodiode falls to zero, while, at the same time, the pressure curve changes its inclination because no longer there is gas production. The pressure at the sharp slope change is defined as the measured PDL value.

Experimental results indicate that the shape factor dramatically affects the propellant PDL. The lowest PDL value is reached when strands of large cross-sectional area (i.e., large shape factor) are used. Two AP/Al/HTPB propellants were tested, featuring the same 68/18/14 mass % composition and AP particle size distribution (0–71 μm), but different Al particle size (μAl or nAl). The results are reported in Fig. 13: the propellant based on nAl has a lower PDL for all shape factors. This effect also suggests that nAl formulations imply a more vigorous energetic coupling at the burning surface in terms of increased heat feedback, thus requiring less assistance from the gas-phase and a self-sustaining burning region more extended toward lower operating pressures.

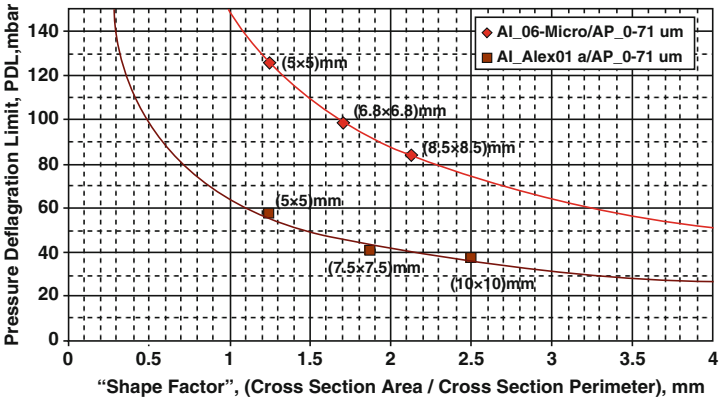

Fig. 13 PDL vs. shape factor for propellants loaded with μAl vs. nAl [56]

3.11 Subatmospheric Burning

Testing the same aluminized propellants of the previous section under subatmospheric pressure revealed another interesting result; for details see [22]. The nAl formulation is not only faster than the μAl formulation but also less pressure sensitive ($n = 0.52$ for nAl and 0.78 for μAl). This finding supports the hypothesis of less dependence of heat feedback from the gas phase to the condensed phase, as indeed expected for nAl formulations. Moreover, while the μAl formulation near PDL shows the typical self-sustained oscillatory burning associated with intrinsic burning instability, this effect is almost unperceivable in the nAl formulation.

3.12 Laser Radiation Ignition

Finally, the ignition delay under laser radiation was evaluated for a number of formulations ranging from 100 % μAl to 100 % nAl and including intermediate mixtures μAl + nAl [37]. Experimental results show a decrease of the ignition delay for nAl loading (propellant P_02) compared to μAl (propellant P_06) with the ignition boundary slope in the range 1.1–1.3; see Fig. 14. Similar results were found by Arkhipov et al. investigating the effects of particle size distribution on radiant ignition [57, 58]. They observed that nAl ignition is "determined by the possibility of rapid oxidation of aluminum powder particles on the burning surface or in the immediate vicinity of it." They also noticed that oxidation of nAl particles may even occur in the heated layer with the flame appearance accompanied by a loud sound effect, surface layer cracking, its fragmentation, and burnout (called "abnormal" ignition regime with heat supply from a heated block). Further effects associated to nAl radiant ignition are described in this book by Zhao et al. [59].

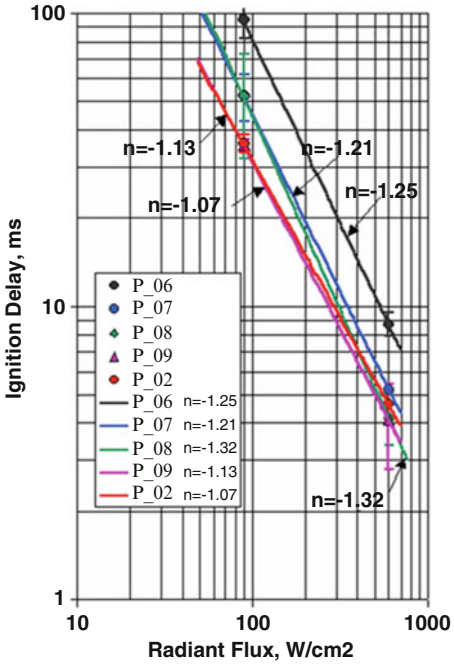

Fig. 14 Radiant ignition map at 1 bar for several AP 68 %/HTPB, 17 % /Al 15 % formulations showing faster ignition for nAl vs. μAl propellants. P_06 is loaded with 100 % μAl flakes; P_07 with 80 % flakes + 20 % nAl; P_08 with 50 % flakes + 50 % nAl; P_09 with 50 % spheres + 50 % nAl; P_02 with 100 % nAl [37]

3.13 nAl Summary

Two different mechanisms, metal agglomeration for μAl and metal aggregation (prompt metal oxidation) for nAl, were underlined. Smaller CCP sizes imply reduced specific impulse losses and also reduced particulate damping especially at low pressures, while the damping effects on high-frequency instabilities require further studies [60]. The exact burning response depends on the details of the propellant formulation: in particular, the pressure exponent of steady burning rates has been observed to follow different trends according to the specifics of the composition and operating conditions. This fact suggests that, in addition to the sheer increase of the specific surface, other subtle chemical and physical factors (intermetallic compounds, crystalline structure, etc.) may be important in nAl enhanced reactivity. At any rate, all burning results may be obscured by cold cohesion phenomena of nAl particles. Modern manufacturing techniques of nanometal powders in general are treated by Vorozhtsov et al. in [61, 62] and, in this book, [63].

A comprehensive review of nAl burning in terms of flame structure and combustion modes was recently offered by Sundaram et al. [64]. Burning rate is controlled by mass diffusion, through the gas-phase mixture, for particle diameters greater than a critical value. The critical particle size decreases from 100–1 μm,

as the pressure increases from 1 to 100 bar, thus making chemical kinetics the controlling factor for nAl combustion over the whole pressure range.

4 Activated μAl Powders

Activation represents a viable solution to the need to increase the reactivity of μAl, preserving its intrinsic qualities. The final product is generally kept micrometric and is characterized by a reduced effect on propellant/solid fuel manufacturing, as well as by a good metal content (higher with respect to nAl). Activation treatments can be divided into three categories according to the selected approach:

- Chemical, when powders are treated through chemical substances (e.g., fluorinated compounds). A number of different techniques are available, depending on the specific activation additive.
- Mechanical, when particles are processed by high- or low-energy mills. One of the most widespread approaches in this category is ball milling, in which the activating action on the powder is executed by a certain number of spheres enclosed in a proper vessel.
- Mechanochemical, when two or more materials are mechanically processed to obtain new substances, like intermetallics. Generally speaking, whenever a process changes the composition or the structure of a powder, the treatment can be considered mechanochemical.

By following different strategies, all of the three activation approaches aim at incrementing the powder reactivity.

4.1 Chemical Activation

Chemical activation (CA) can be used to increase the specific surface area of micron-sized powders or to deposit substances, like fluorinated compounds or transition metals, which can increase reactivity on the particle surface. The increment of the particle S_{sp} based on a pitting corrosion procedure, using a solution of water and magnesium chloride, was successfully tested by Rosenband and Gany in [65]. The resulting S_{sp} value, higher than that of standard μAl and similar to that of nAl (10–18 m^2/g), guaranteed a good increase of powder reactivity [65, 66]. A widespread strategy, described in [65, 67, 68], consists in activating Al particles by deposition of metals (such as Ni, Co, and Fe) and complex fluoride compounds. In the latter case, the activation strategy consists in reducing the distance between particles and additive. When complex fluorides are used, the weakening of the protective alumina shell also occurs, promoting a faster diffusion of oxidizer towards the Al core [67, 69].

Chemical treatment processes do not modify particle shape. However, the deposition of the activation substance can alter the superficial texture (see Fig. 15)

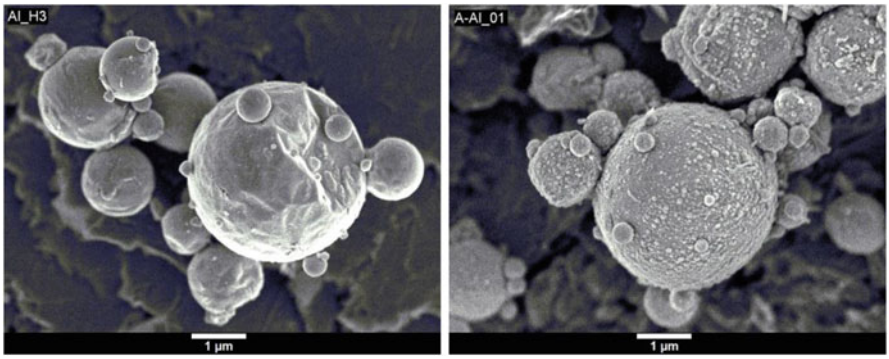

Fig. 15 Standard μAl particles before (*left*) and after (*right*) a chemical activation treatment with complex fluoride

Table 4 Effect of different chemical activation treatments using complex fluoride on powder specific surface area, size, and metal content

ID	Ref. powder	CA-Me	CA-Lo	CA-Hi
Activation intensity	None	Medium	Low	High
D_{43}, μm	5.1	5.5	5.4	5.5
S_{sp}, m^2/g	1.2	2.6	2.2	2.3
Metal content, %	98.3 ± 0.7	93.9 ± 0.9	93.7 ± 0.5	90.5 ± 0.5

with a consequent variation of both the specific surface area and mass-weighted mean diameter of the particles. The effect of a chemical treatment using complex fluoride can be appreciated in Fig. 15, but the exact effect on powder characteristics depends on the specific activation procedure, as reported in Table 4. The metal content, for example, is affected by the activation treatment with a progressive reduction related to the selected additive and to the process duration. In the case of Al activated with a complex fluoride, the metal content depletion is of the order of 5–8 % by mass.

4.2 Mechanical Activation

Mechanical activation aims at incrementing particle reactivity by several ways:

- Particle shape variation
- Additive inclusion, by ball milling techniques
- Distance reduction between particles and additive, for example, employing mechanical mixing techniques

Mechanical milling (MM) is an activation technique consisting in grinding one or more powders by low- or high- energy mills (centrifugal, planetary, or attritor). This approach can be used to produce a series of ingredients, like amorphous powders

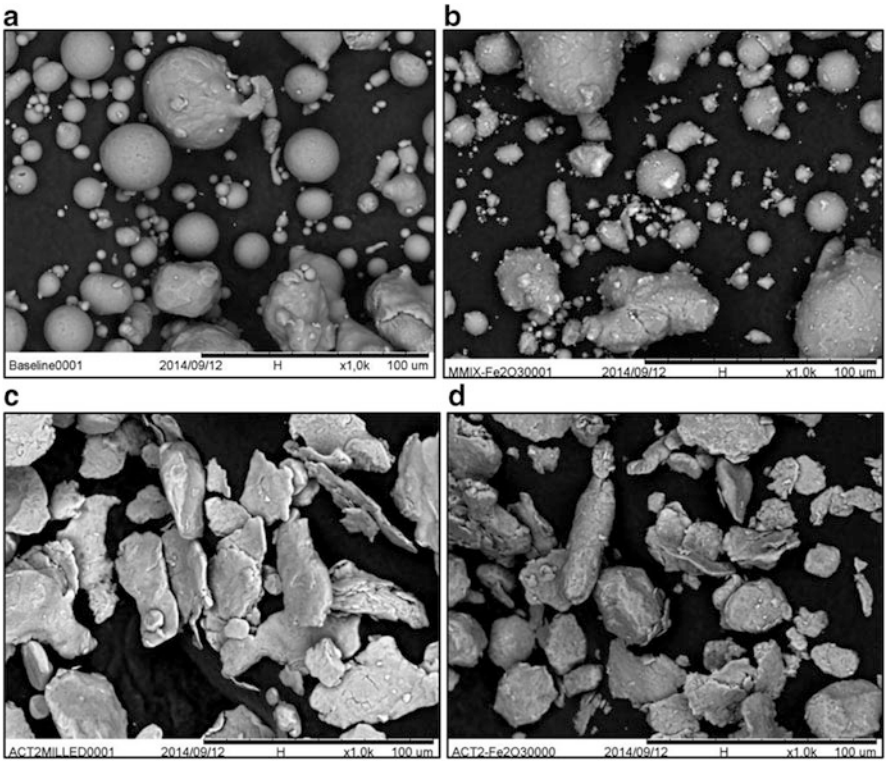

Fig. 16 Effects of different kinds of mechanical activation on a reference μAl. (**a**) Reference Al 30 μm (**b**) Mechanical mixing with Fe_2O_3 (**c**) Mechanical milling (**d**) Mechanical milling with Fe_2O_3

and metal–ceramic composites, or to change the structure of materials [70, 71]. In these cases, the activation is of mechanochemical type. From the standpoint of increasing the effectiveness of aluminum as a propellant fuel ingredient, the most interesting advantage of MM is represented by the enhanced reactivity of the final product, evidenced by a reduction of both ignition temperature and activation energy [72–74]. As with chemical activation, MM leads to a metal content reduction of about 1–2 % for a standard μAl [74]. This loss is associated with the exposure of the Al core to the external environment and is imputable to deformations induced by mechanical stresses applied to particles during the activation treatment. A further loss of elemental metal content is prompted by the presence of an additive, generally added in high mass fractions (10 % or more). The cumulative loss also depends on a series of parameters, like milling time, atmosphere, ball-to-powder mass ratio (BPR), and process control agent (PCA). PCA, in particular, is important to reduce particle–particle and particle–sphere cold welding phenomena. MM strongly affects particle shape and surfacetexture as shown in Fig. 16c, d as compared to Fig. 16a

Table 5 Effect of mechanical activation treatments on powder metal content (volumetric method [28])

ID	μAl-30 μm	MM	MM-Fe_2O_3	MMx-Fe_2O_3
Activation	None	Ball milling	Ball milling	Mech. mix
Metal content, %	99.3 ± 0.2	97.5 ± 0.4	94.0 ± 0.9	96.7

Table 6 Ignition temperature for different kinds of activated Al. Two μAl and a 100 nm nAl coated with stearic acid are reported for comparison

ID	Ignition	Ignition temperature, K
μAl – 5 μm	Yes	1155.2 ± 18.0
μAl – 30 μm	No	–
CA – Lo	Yes	870.7 ± 14.5
CA – Me	Yes	904.8 ± 16.2
CA – Hi	Yes	859.0 ± 11.0
MM	[a]	–
MM with Fe_2O_3	Yes	876.4 ± 12.8
nAl	Yes	771.3 ± 16.3

[a]The specific MM treatment strongly influences this parameter

(reference μAl). Activated powders are characterized by flake-shaped particles and by an irregular external surface. The additive, if present, tends to be entrapped in the granules (see Fig. 16d).

The possibility of activating μAl by mechanical mixing using a low amount of additive (mass fraction < 5 %) has recently been investigated by Dossi [75]. The treatment is capable of retaining the original granule shape and is accomplished using nanometric additives to promote efficient particle coating. Except for some spots, the additive distribution on Al granule surface is homogeneous (Fig. 16b). The treatment promoted an interesting increment of particle reactivity and provided a higher metal content compared with the corresponding powders processed by ball milling (see Table 5).

4.3 Effects of Activation Processes on Powder Reactivity

The capability of mechanical and chemical activation of increasing particle reactivity has been investigated through ignition and TG analyses. A lowering of the ignition temperature has been detected for both chemically and mechanically activated powders, confirming the benefits of these treatments (Table 6). The mechanical treatment brings to a stronger ignition temperature reduction compared with chemical process.

TG traces reported in Fig. 17 confirm what was observed in terms of ignition temperature changes for mechanically activated powders. Milled powders show a significant mass gain in the thermal region of the first oxidation step. Conversely, the ingredient treated with mechanical mixing shows a marked mass increment only during the second oxidation step. At high temperature, the mass gain obtained by

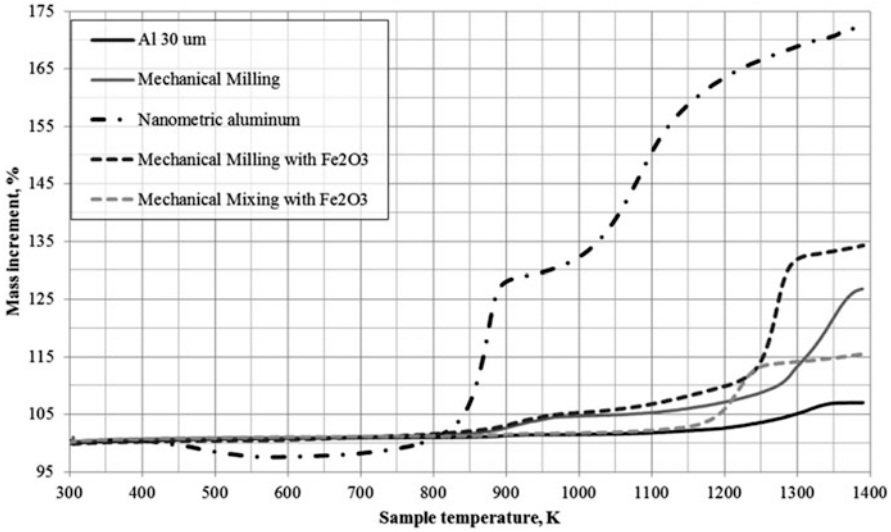

Fig. 17 TG analyses for three mechanically activated Al powders (sample mass: 2 mg; atmosphere: air; heating rate: 10 K/min). The reference Al and a 100 nm nAl coated with stearic acid are reported for comparison

mechanically milled powders is higher than that seen with mechanically mixed ingredients. In this respect, particle morphology variation may play a significant role. Despite a generalized enhancement, all the activated Al materials are characterized by a lower reactivity than nAl as confirmed by the lower mass gain and the delayed oxidation step onsets.

TG analyses of ingredients activated with complex fluoride show an increment of reactivity that is generally higher compared with that shown by mechanically activated powders. However, differences in test parameters and grain size distribution of the reference powder have to be considered. A single major mass gain is located around the Al melting point and is delayed by about 100 K with respect to the onset shown by the μAl-05 powder (Fig. 18). Both mechanical and chemical activation processes are not able to achieve the same results obtained by nAl despite an evident reactivity increment.

4.4 Potentialities of Activated Al Powders in Solid Rocket Propellants

The high reactivity of activated Al can bring about a reduction of condensed combustion product (CCP) size, as shown by Yavor et al. [66], Dossi [75], and Sippel et al. [76], leading to a potential reduction of solid rocket motor performance losses. This possibility is accomplished only if the metal content of the selected

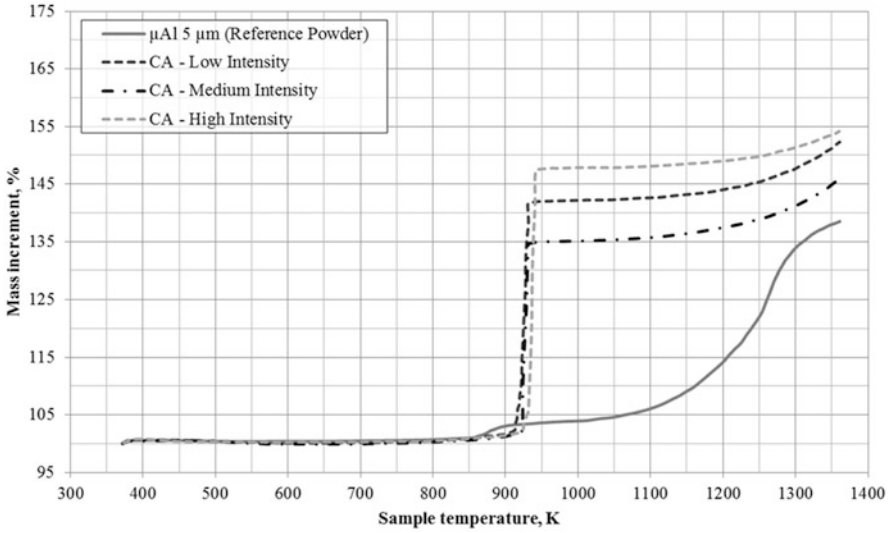

Fig. 18 TG analyses for three chemically activated Al with complex fluoride (sample mass: 9–12 mg; atmosphere: O_2; heating rate: 40 K/min). The reference Al is reported for comparison

Al powder is sufficiently high. In fact, a reduction of Al content of about 15 % is sufficient to jeopardize the performance gain obtainable by eliminating the agglomeration phenomena. Figure 19 shows the ideal I_s calculated for AP/HTPB-based propellants incorporating different metals. The use of activated powders always implies a I_s reduction, but their active Al content guarantees a higher ideal I_s value with respect to nAl. Ingredients processed by MM techniques using a low amount of additive provide a higher I_s value than chemically activated ingredients, approaching that obtained by µAl.

When incorporated into solid propellants, activated ingredients result in an enhancement of the burning rate as shown in Fig. 20. In this respect, mechanically activated powders seem more effective than chemically activated ingredients. However, the positive effect caused by the specific additive (iron oxide) has to be considered. Chemically activated powders provide virtually the same burning rate increment, independent of the treatment intensity. Conversely, the choice of the specific mechanical process seems to control the effect of the powder on the solid propellant burning rate. MM-Fe_2O_3 and MMx-Fe_2O_3, for example, assure a very strong enhancement, similar to nAl or even higher. The effect of particle morphology variation can be observed in the P-MM propellant test results, showing the same burning rate of P-µAl-05 loaded with standard 5 µm Al. The pressure sensitivity is also affected by the activation treatment. Ingredients processed by CA are responsible for an increased propellant pressure exponent, while mechanically activated powders tend to reduce the ballistic exponent or to keep it unaltered. The exact effect depends on the specific ingredient and the precise mechanical activation treatment.

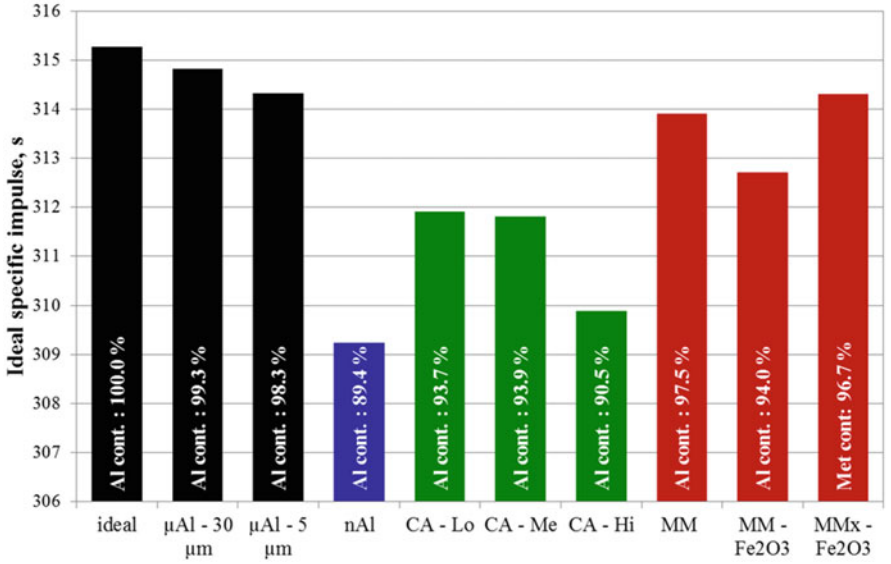

Fig. 19 Effect of different metal powders on ideal specific impulse of AP/Al/HTPB – 68 %/18 %/14 % (in mass) solid propellants. Computations are performed considering a combustion chamber pressure of 70 bar, an expansion ratio of 40, and vacuum conditions

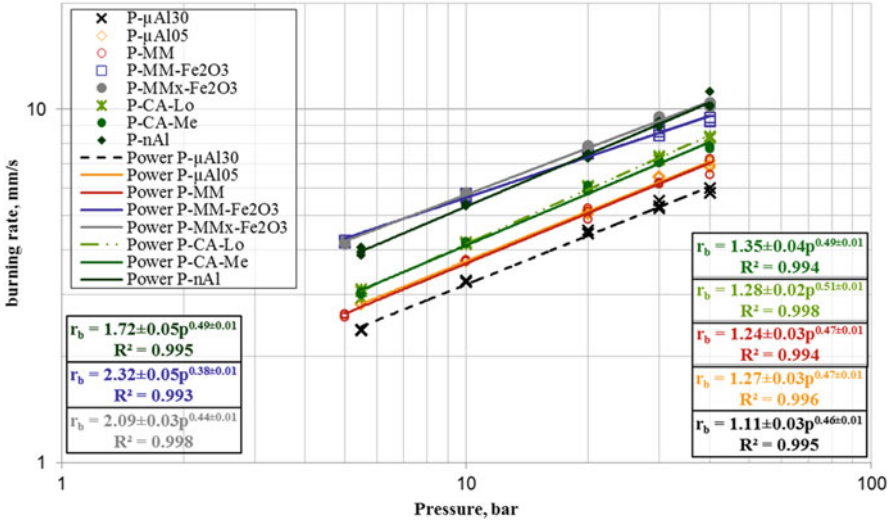

Fig. 20 Effect of different metal fuels on steady burning rate of AP/Al/HTPB – 68 %/18 %/14 % (in mass) solid propellants [56]

5 MgB Dual-Metal Powders

Boron has the highest theoretical energy density (~59 kJ/g) among the metal or metalloid fuels, with little toxicity and no reactivity issues (such as for Be or Li). This fact makes B a very attractive ingredient for energetic applications. But combustion difficulties (recalled in section "Thermochemical properties") and a reduction up to 5 % of I_s [77] for propellant formulations containing B in place of Al metal conspire to keep B out of solid rocket propellants. Among the many techniques proposed to make B a useful ingredient, a promising one is to resort to dual Al and B metal fuels [77, 78]. In this respect, several Mg_xB_y composite dual-metal powders were tested under laboratory conditions differing by the Mg coating amount (ranging from 10 to 60 % in mass) and B purity. By ICP bulk elemental analysis, boron purity was either 90 % (typically 90–91 % with 5 % max Mg impurity) or 95 % (typically 96 % with 1 % max Mg impurity) and the balance being in both cases oxygenated impurities, moisture, and volatiles. For completeness, pure boron powders were also examined. The theoretical ideal I_s, as well as the adiabatic flame temperature, decrease whenever Al is replaced, totally or partially, by B, Mg, or Mg_xB_y composite metals. A good strategy appears that of a partial replacement, say 3 % of μAl (one sixth of the total μAl load for a standard composite propellant for space propulsion).

Visual inspections of the collected SEM images of the tested metal powders show that Mg_xB_y powders appear larger than the corresponding pure B powders and that 95 % purity B powders appear larger than the corresponding 90 % purity B powders. In addition, all of the tested B powders present an irregular shape different from the near spherical μAl used as a reference metal fuel. B powders present fine particles with no significant cohesion; Mg_xB_y powders feature monomodal distributions with typically $D_{43} \approx 5$ μm, with the exception of $Mg_{60}B_{40}$ ($D_{43} = 20.9$ μm). While Mg_xB_y with 90 % B purity presents no significant cohesion, Mg_xB_y with 95 % B purity may occasionally display visible clumps.

The structure of each Mg_xB_y particle, by X-ray ablation methods, consists of a center of the original Boron input material with a shell of intermetallic material Mg_xB_y which is richer in Magnesium nearest the surface. The approximate surface composition is MgB_2, a brown material which is visually indistinguishable from Boron.

Particle size distributions analyses point out that the tested metal powders tend to pack and stick together into clumps. This trend increases with time, if proper care is not taken during powder storage. But the clumps can be removed by applying a shear stress above some threshold value.

For the listed B_{90}-based dual-metal formulations, Fig. 21 shows that the addition of Mg_xB_y composite metal powders leads to a measurable increase of steady burning rate with respect to the μAl baseline, but not the pure B_{90} baseline. For the tested B_{95}-based formulations, experimental results (not shown) point out that the addition of Mg_xB_y composite metal powders leads to an even more observable increase of steady burning rate with respect to both the μAl baseline and also the pure B_{95}

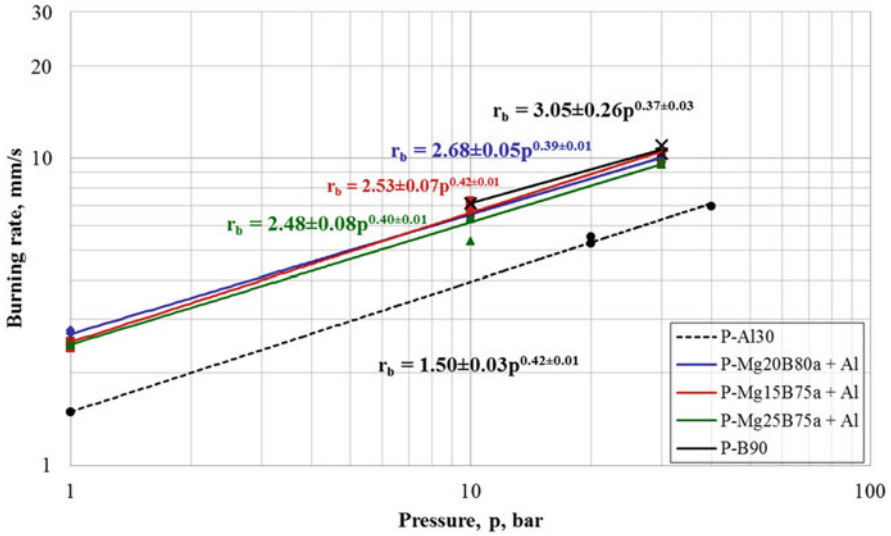

Fig. 21 Comparing steady burning rates of B90-based dual-metal solid propellants: Mg_xB_y addition yields an appreciable increase with respect to the μAl baseline but not with respect to the B90 baseline [81]

baseline. In both cases, the precise content of Mg coating in the range 10–25 % has a minor effect on the propellant burning rate. However, for increasing Mg content, the burning rate gain fades away, for example, when Mg addition reaches 60 %.

Tests to evaluate the incipient agglomeration phenomena were performed under N_2 atmosphere at 5, 10, 20, and 25 bars; some tests were repeated in Ar without noticeable changes. Combustion was performed in a strand burner, recorded by a high-resolution and high-speed video camera for slow motion post-processing and later analyzed with graphic software. For each test, the size of 200 incipient agglomerates was manually measured and the D_{43} mean diameter was then calculated. For all experimental series, the minimum diameter distinctly observable was around 30 μm. As an example, the results obtained for the listed B_{90}-based dual-metal formulations are illustrated in Fig. 22, pointing out a general decrease of the average agglomerate size, especially for 25 % Mg coating.

Ignition temperature of all tested powders was evaluated at SPLab through a specially designed experimental apparatus in air at 1 bar [79]. The ignition temperature is below 800 K for the nAl tested in this work (see Table 6), while for B it is estimated around 1900 K for single particles [78] and down to 1200 K for agglomerates [80]. Further experimental data collected at SPLab [81] point out the beneficial effect of Mg in lowering the Mg_xB_y ignition temperature to the level of nAl.

Comparing the ignition temperature of the tested metal powders with the corresponding adiabatic flame temperature of the pocket at the same pressure, with the metal fuel assumed chemically inert, one observes that the propellant microstructure temperature can be appreciably higher than that of the metal powder

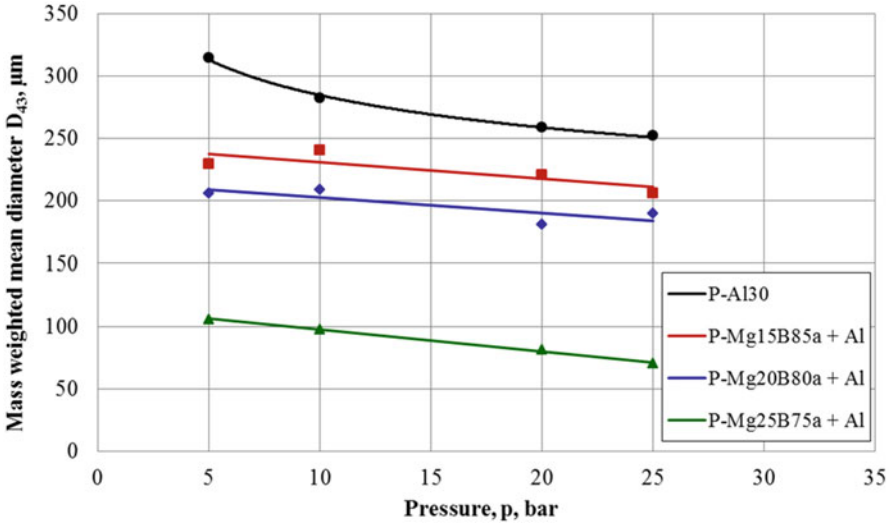

Fig. 22 Average agglomerate size D_{43} vs. pressure of the indicated B90-based dual-metal solid propellants: Mg_xB_y addition with 15–25 % Mg coating causes a general decrease of the average agglomerate size, especially for 25 % Mg coating [81]

ignition. The local exothermicity is then sufficiently high to promote ignition of the metallic powders and induce at least a partial participation in the combustion process, thus strongly increasing the pocket adiabatic flame temperature.

A basic role in these phenomena is played by the propellant microstructure. In general, the conductive thermal wave preceding the burning surface, possibly augmented by exothermic reactions, is able to warm up the metal particles dispersed within the propellant microstructure to temperatures high enough to trigger ignition and a partial oxidation of the metal particles. The intimate mixing with the surrounding decomposition products of the fine AP fractions and binder, favoring a local under-oxidized premixed flame, promotes the formation of partially oxidized and intermediate metallized thin flakes (prompt metal oxidation).

The combination of low metal particle ignition temperature and high pocket adiabatic flame temperature favors at the same time high burning rates (Fig. 21) and small size agglomerates (Fig. 22). Propellant samples containing Mg_xB_y powder with 10–25 % Mg are characterized by high pocket adiabatic flame temperatures and also by low metal particle ignition temperatures. These samples show low values of the incipient agglomerate D_{43} size. In particular, a composite formulation partially replacing µAl with Mg_xB_y at 25 % Mg showed the strongest reduction of the incipient agglomerate mean size with respect to the µAl baseline (72 % at 25 bar in Fig. 22).

Whereas all of the tested propellant formulations containing micrometric Al produce agglomerates (spherical drops of liquid metal and alumina in combustion with a distinct oxide cap), no clear agglomeration phenomena could be detected for the propellant formulations containing only the B compounds under examination.

Even if agglomeration occurs, generating burning drops below the optical system resolution or outside the optical system field of view, the combustion process of the B compounds is essentially characterized by the formation of thin flakes (sintered fractal aggregates in the description of [77]).

Depending on steady-state burning rate (i.e., pressure), the type of binder, fine oxidizer size and fraction, metal average size, and distribution, unburned metal may also contribute to the thin flake formation.

6 Comparing Different Metal Powders

A negative effect of Al burning is due to the generation of an appreciable mass fraction of condensed products (ξ_{cc}). The condensed species, originated from the propellant metal particle combustion, are responsible for the two-phase flow losses which cause a downward departure from ideal motor performance. The delivered specific impulse undergoes a few % reduction, due to the interaction between the continuous gas phase and the dispersed phase. Losses are concentrated at the nozzle throat and are only partially recovered during the supersonic expansion; for example, see [22, 82].

6.1 Ballistic Properties

The effects of three different kinds of Al powders on the propellant ballistic properties have been compared in terms of burning rate value and combustion residue size. Regarding particle size distribution, a comparison among a standard μAl powder (μAl-30, 30 μm, spherical shape), a nAl (ALEX, spherical shape) and a mechanically activated Al (MM) is shown in Fig. 23.

Burning rate was evaluated in a standard window strand burner by a high-speed video camera; for details, see [22]. Likewise, condensed combustion products (CCPs) were quenched and collected in a pool filled with tetrachloroethene, in a burner using the same operating conditions (ignition, pressurizing gas, etc.) used for steady burning rate measurements; for details, see [22].

Table 7 shows the main features of the compared Al powders. Particle size distributions are shown in Fig. 23. The results of burning rate evaluations are reported in Table 8, expressed according to Vieille's law ($r_b = ap^n$) over the tested pressure range 10–40 bar. Concerning combustion residuals, a test campaign was

Table 7 Raw Al powder characteristic comparison [83]

ID	Description	D_{43} μm	Metal content (%)
nAl (ALEX)	Nanometric, spherical, uncoated	0.14	88.7
μAl-30	Micrometric, spherical, uncoated	42.66	99.5
MM	Micrometric, milled	65.02	97.7

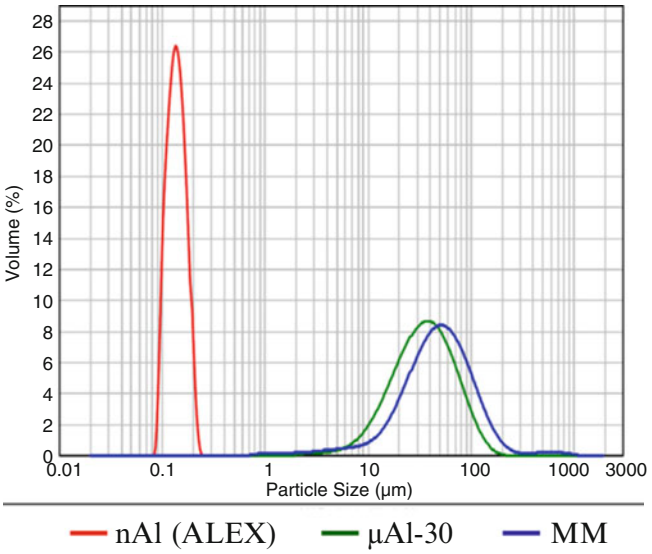

Fig. 23 Particle size distributions of the three metal powders compared. Analyses conducted with a laser granulometer Malvern Mastersizer 2000 using the Hydro unit

Table 8 Steady burning rates results [75, 83]

ID	a, (mm/s)/bar^n	n	R^2
P-nAl (ALEX)	1.68 ± 0.03	0.50 ± 0.01	0.999
P-μAl-30 μm	1.11 ± 0.03	0.46 ± 0.01	0.995
P-MM	1.24 ± 0.03	0.47 ± 0.01	0.994

conducted to evaluate the particle size with respect to pressure (10 and 30 bar), and an XRD analysis was conducted to identify the phases present in the collected samples.

Table 9 shows the X-ray diffraction (XRD) analysis results. The phases detected are aluminum (Al^0) and aluminum oxide (α-Al_2O_3, γ-Al_2O_3, δ*-Al_2O_3). The phase δ*-Al_2O_3 is typically formed following a violent quenching process of liquid alumina. Aluminum combustion efficiency, defined as the ratio Al_2O_3/Al^0, highlights the different behavior of nAl and μAl powders: over the limited pressure range explored, for increasing pressure it decreases for nAl, while it increases for μAl [83].

In agreement with previous works [79], nAl with respect to μAl increases not only burning rate but also combustion efficiency (see Table 9 and Fig. 24) and moreover makes CCP size smaller. Likewise, the tested milled Al shows better performance than the standard spherical μAl [75, 83].

Table 9 XRD analysis results [75, 83]

ID	p, bar	Al^0, %	α-Al_2O_3, %	γ-Al_2O_3, %	δ*-Al_2O_3, %	Al_2O_3/Al^0
P-nAl (ALEX)	10	0.3	2.6	76.6	20.5	332.3
	30	0.8	3.8	78.4	17.0	124.0
P-μAl-30	10	22.2	2.7	58.8	16.3	3.5
	30	12.3	2.3	67.5	17.9	7.1
P-MM	10	15.6	4.4	61.3	18.7	5.4
	30	8.0	1.4	67.5	23.1	11.5

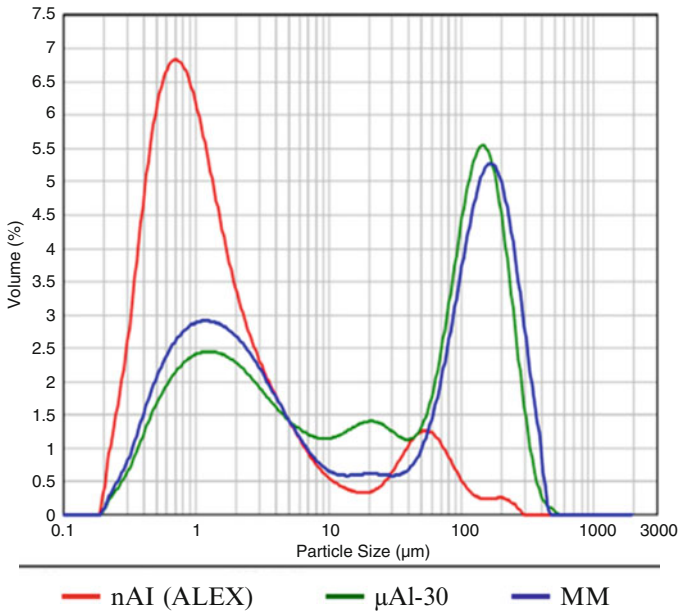

Fig. 24 Particle size distribution of CCP collected at 30 bar. Analyses conducted with a laser granulometer Malvern Mastersizer 2000 using the Scirocco unit

7 Concluding Remarks

Under the common operating conditions tested at SPLab, typical of space propulsion applications, the following trends are observed:

- Concerning nAl ($\rho = 2.520$ g/cm^3), a slight loss of ideal I_s is expected compared with μAl due to decreased active metal content; steady burning rates can increase up to a factor of 2; incipient agglomeration is decreased.
- Concerning Mg_xB_y dual metals ($\rho = 1.450$ g/cm^3), a slight loss of both ideal I_s and density is expected with respect to μAl; steady burning rates can increase up to a factor of 3 with 95 % purity B; incipient agglomeration is strongly decreased.

- Concerning AlH_3 ($\rho = 1.476$ g/cm^3), although not commercially available and in spite of its low density, this hydride shows a substantial increase of ideal I_s for both solid and hybrid rocket propulsion. It also features a unique combination of a mild to strong increase of burning rates with a significant decrease of pressure sensitivity; incipient agglomeration is mildly decreased.
- Concerning actAl (ρ variable around that of pure Al, depending on the type and amount of additives), a small increment of the delivered I_s is expected with respect to standard μAl due to good active metal content level combined with appreciable reduction of CCP size.

In terms of industrial applications, no substitute for standard μAl is in use for rocket propulsion. Concerning nAl, extensive experimental and theoretical research activities were carried out internationally covering a variety of energetic applications, including propellants, pyrotechnics, and explosives. After more than 30 years of investigations, no operational systems are reported in use for nAl powders. Loss of active metal; occurrence of cold cohesion or clustering during manufacture, storage, and handling; increased slurry viscosity; possible interactions with the binder system; and so on clearly overcome advantages such as increased burning rate (easily achievable in other ways) and possible reduction of 2P flow losses. Likewise, no operational systems are in use for activated Al and Mg_xB_y metals.

Concerning AlH_3, an overall assessment appears somewhat elusive. This hydride appears suitable to SRM upper stages and hybrid propulsion in general [84, 85], but no use of it is officially reported. Under low heating rates, AlH_3 dehydrogenation temperature is in general around 433 K, while it was measured at 452.7 K for the Russian product, which is anyway much less than the decomposition temperatures of the common binders. Even under combustion tests, this difference brings about a porous metallic structure in the composite propellant matrix, which in turn makes micrometric Al much more reactive by increasing its specific surface area. Details about AlH_3 ignition (in terms of 2 % maximum light emission) and combustion properties are discussed in [86–88]. Testing at heating rates of 1×10^5 K/s in air, for pressures ranging from atmospheric to about 70 bar, indicates that the dehydrogenation temperature of 720 K of aluminum hydride is independent of pressure. On the contrary, the ignition temperature is approximately linearly decreasing from the value of 900 K at atmospheric pressure to about 760 K at 4 bar; above 4 bar it maintains approximately constant with an average value of 760 K. The important message is that the ignition temperatures of AlH_3 fall in the same low range values typical of nAl (see Table 6), thus confirming the positive effects of the porous metallic structure created by fast dehydrogenation. In turn, these low ignition temperatures eliminate the relatively large standoff distance observed for μAl particle burning in the currently employed metallized formulations. Ultimately, this leads to an appreciable burning rate increase and incipient agglomeration decrease.

While ideal thermochemistry favors Al ($\rho = 2.700$ g/cm^3) as the most suitable metal fuel in terms of gravimetric specific impulse, considerations of the

generated CCP amount and average size point out other promising directions for enhancing the actually delivered specific impulse. The well-known agglomeration phenomena, observed near the burning surface (incipient agglomeration) in the combustion of μAl particles, are drastically modified for some of the evaluated dual-metal formulations. For propellant microstructures using nAl or Mg_xB_y as metallic ingredients, visual inspections of the near burning surface region point to aggregation phenomena (prompt oxidation), without the typical transition to agglomeration, which go much beyond the simple reduction of the particle ignition standoff distance. This essentially heterogeneous burning mechanism yields larger steady-state burning rates and smaller agglomerates of unusual structure, consisting for nAl of a central metal core surrounded by an oxide layer (see Fig. 9d). Both phenomena can be ascribed to the combined effects of large specific surface and low ignition temperature of the metal fuel. Subsurface heating is provided by the conductive thermal wave in the condensed phase, with the possible augmentation by the exothermic reactions of the local premixed flame.

Thus, as of this writing, the recommended approach is to address the attention to dual-metal formulations (μAl–nAl, μAl–Mg_xB_y, etc.) and to identify the optimum compositions, leading to improved ballistic properties under real operating conditions. In particular:

- For μAl–nAl dual-metal formulations, best results are obtained with a partial replacement, around 20–30 % mass of μAl.
- For μAl–Mg_xB_y dual-metal formulations, best results in terms of reduced average agglomerate size are obtained with 25 % Mg coating, while 60 % Mg coating leads to a measurable decrease of steady burning rate.
- For μAl–actAl (either chemically or mechanically) dual-metal formulations, optimization studies are under way and not yet conclusive. However, preliminary studies suggest that actAl powders are a good candidate only for a complete substitution of μAl, if good packing and mechanical properties can be maintained. According to the experimental campaigns executed in past years, μAl–actAl dual formulations are not effective in significantly changing both the burning rate and the agglomerate size of standard aluminized AP-/HTPB-based solid rocket propellants.

Overall, it can be said that the chemistry and physics of the microstructure are important in understanding and controlling the propellant combustion properties and ultimately flight performance. At least two new directions recently appeared capable of drastically modifying, in the long range, the current understanding of metal burning. The first contribution is due to Glorian et al. [89]. Since the Al combustion chemistry in the gas phase is quite well known even under propellant burning conditions, they focused their attention on the elusive details of the combustion chemistries at the surface and surface/gas interface. Depending on the Al particle size especially and a number of additional parameters as well, these chemistries may exert important effects to the overall combustion process. The combustion of nAl in particular (switching from a diffusive to a premixed flame) appears more sensitive to surface reactions than μAl particles. In this respect, surface reactions in

general were carefully studied by quantum chemistry. Basic heterogeneous kinetics describes how molecules interact with metallic surfaces: the first step is adsorption (chemisorption), that is the binding of the adsorbate (atom, radical, molecule) with one or more atoms on the surface. In the pioneering work [89], small adsorbates on Al, such as atoms, were studied experimentally, these species being the simplest intermediates. Adsorption sites, vibrational frequencies, and thermodynamic properties of adsorbed species on an Al surface were calculated using a parameterized density functional method. In spite of a severe lack of experimental information, thermochemical data and kinetic data were developed that can be used to specifically assist modeling surface reactions of Al particle combustion. Considerable efforts are still needed to model the combustion chemistry under the complex operating conditions of segmented solid rocket motors. Eventually, this approach may open the path to a new and more comprehensive understanding of Al and, more generally, metal burning.

An even more drastic prospect is that opened by Komarov and Shandakov [90]. In a thermochemical study conducted under very general conditions, they show that it is possible in principle to get high (computed) I_s by totally avoiding the use of metals or hydrides. The authors show that the basic role of metals or hydrides is simply that of increasing the flame temperature. In the region of oxidizers with a negative heat of formation Δh_f^0, the role of the metal or hydrides in increasing I_s is substantial. But moving into the region of oxidizers with positive Δh_f^0, the role of the metal or hydrides in increasing I_s becomes smaller and may even cause it to decrease! Therefore, by properly combining oxidizers with large enough heats of formation and energetic binders, one can achieve a remarkable I_s increase, compared with current technologies, without the penalties imposed by the use of metals and chlorine (when AP is used as oxidizer); for details see also [91] in this book.

References

1. Williams FA, Barrère M, Huang NC (1969) Fundamental aspects of solid propellant rockets. Technivision Services, Slough, UK. AGARDograph. AGARDograph 116
2. Sakovich GV (1995) Design principles of advanced solid propellants. J Propuls Power 11(4):830–837
3. Maggi F, Gariani G, Galfetti L et al (2012) Theoretical analysis of hydrides in solid and hybrid rocket propulsion. Int J Hydrog Energy 37:1760–1769. doi:10.1016/j.ijhydene.2011.10.018
4. DeLuca LT, Maggi F, Dossi S et al (2013) High-energy metal fuels for rocket propulsion: characterization and performance. Chin J Explos Propellants 36:1–14
5. Karabeyoglu A (2016) Chapter 5: Performance additives for hybrid rocket engines. In: DeLuca LT, Shimada T, Sinditskii VP, Calabro M (eds) Chemical rocket propulsion: a comprehensive survey of energetic materials. Springer International Publishing, Cham
6. Risha GA, Evans BJ, Boyer E, AIAA et al (2007) Metals, energetic additives, and special binders used in solid fuels for hybrid. In: Chiaverini MJ, Kuo KK (eds) Fundamentals of hybrid rocket combustion and propulsion. AIAA, Reston, pp 413–456
7. Gromov AA, Teipel U (eds) (2014) Metal nanopowders: production, characterization, and energetic applications. Wiley-VCH, Weinheim
8. Anon. (1993) Beryllium and beryllium compounds (No. 58), IARC summaries & evaluations. International Agency for Research on Cancer (IARC)

9. Srivastava RD, Farber M (1978) Thermodynamic properties of Group 3 oxides. Chem Rev 78:627–638. doi:10.1021/cr60316a002
10. Chase MWJ (1998) NIST-JANAF thermochemical tables. J Phys Chem Ref Data 9:1–1951
11. Haddad A, Natan B, Arieli R (2011) The performance of a boron-loaded gel-fuel ramjet. In: DeLuca LT, Bonnal C, Frolov S, Haidn OJ (eds) Progress in propulsion physics. EDP Sciences, Paris, pp 499–518. doi:10.1051/eucass/201102499
12. DeLuca LT, Marchesi E, Spreafico M et al (2010) Aggregation versus agglomeration in metallized solid rocket propellants. Int J Energy Mater Chem Propuls 9:91–105
13. Navrotsky A (2003) Energetics of nanoparticle oxides: interplay between surface energy and polymorphism. Geochem Trans 4:34–37. doi:10.1039/b308711e
14. Gromov AA, Maggi F, Malikova EV et al (2014) Combustion synthesis of AlN (Al3O3N), BN, ZrN, and TiN in air and ceramic application. In: Gromov AA, Chukhlomina LN (eds) Nitride ceramics: combustion synthesis, properties and applications. Wiley-VCH, Weinheim, pp 125–163
15. Kubota N (2007) Propellants and explosives: thermochemical aspects of combustion, 2nd edn. Wiley-VCH, Weinheim
16. Lide DR (2007) CRC handbook of chemistry and physics, 88th edn. CRC Press, Boca Raton
17. Glassman I (2008) Combustion, 4th edn. Academic Press/Elsevier, New York
18. Perry RH et al (1997) Perry's chemical engineers' handbook, 7th edn. McGraw Hill, New York
19. Dean JA (1999) Lange's handbook of chemistry, 15th edn. McGraw Hill, New York
20. Gen MY, Frolov YV, Storozhev VB (1978) On combustion of particles of subdispersed aluminum. Combust Explosion Shock Waves 14(5):153–155
21. Gen MY, Ziskin MS, Petrov YI (1959) Investigation of aluminum aerosol dispersion depending on of their formation conditions. Proc Acad Sci USSR (Doklady) 127:366
22. DeLuca LT, Galfetti L, Maggi F et al (2014) Chapter 12: Characterization and combustion of aluminum nanopowders in energetic systems. In: Gromov AA, Teipel U (eds) Metal nanopowders: production, characterization, and energetic applications. Wiley VCH, Wenheim, pp 301–400
23. Kwon YS, Jung YH, Yavorovsky NA et al (2001) Ultra-fine powder by wire explosion method. Scr Mater 44(8–9):2247–2251
24. Advanced Powder Technologies LLC (2015) http://www.nanosized-powders.com. Accessed 31 Mar 2015
25. Kwo YS, Gromov AA, Strokova JJ (2007) Passivation of the surface of aluminum nanopowders by protective coatings of different chemical origin. Appl Surf Sci 253:5558–5564
26. Sossi A, Duranti E, Paravan C, DeLuca LT, Vorozhtsov AB, Gromov AA, Pautova YI, Lerner MI, Rodkevich NG (2013) Non-isothermal oxidation of aluminum nanopowder coated by hydrocarbons and fluorohydrocarbons. Appl Surf Sci 271:337–343. doi:10.1016/j.apsusc.2013.01.197
27. Sossi A, Duranti E, Manzoni M, Paravan C, DeLuca LT, Vorozhtsov AB, Lerner MI, Rodkevich NG, Gromov AA, Savin N (2013) Combustion of HTPB-based solid fuels loaded with coated nanoaluminum. Combust Sci Technol 185(1):17–36. doi:10.1080/00102202.2012.707261
28. Chen L, Song W, Lv J et al (2010) Research on the methods to determine metallic aluminum content in aluminum nanoparticles. Mater Chem Phys 120:670–675
29. Klager K (1984) Polyurethanes, the most versatile binder for solid composite propellants. Am Inst Aeronaut Astronaut. doi:10.2514/6.1984-1239
30. Humble R (2000) Fuel performance enhancements for hybrid rockets. Am Inst Aeronaut Astronaut. doi:10.2514/6.2000-3437
31. Mackay ME, Tuteja A, Duxbury PM et al (2006) General strategies for nanoparticle dispersion. Science 311:1740–1743
32. Reina A, Paravan C, Morlacchi M, Frosi A, Maggi F, DeLuca LT (2013) Rheological and mechanical behavior of coated aluminum loaded nano-composites. In: Haidn OJ, Zinner W, Calabro M (eds) 5th European conference for aerospace sciences (EUCASS 2013), ISBN: 9788494153105, pp 1–14 [5th European conference for aerospace sciences (EUCASS 2013), Munich 1–5 Jul 2013]

33. Zare A, Harriman T, Lucca DA, Roncalli S, Kosowski BM, Paravan C, DeLuca LT (2016) Chapter 27: Mapping of aluminum particle dispersion in solid rocket fuel formulations. In: DeLuca LT, Shimada T, Sinditskii VP, Calabro M (eds) Chemical rocket propulsion: a comprehensive survey of energetic materials. Springer International Publishing, Cham
34. Pokhil PF, Belyaev AF, Frolov YV (1972) Combustion of Metal Powders in Active Media. Nauka, Moscow
35. Price EW (1979) Combustion of aluminum in solid propellant flames, AGARD PEP 53rd Meeting on solid rocket motor technology, Paper 14, AGARD, Paris
36. Price EW (1984) Chap. 9: Combustion of metallized propellants, fundamentals of solid propellants combustion. In: Kuo KK, Summerfield M (eds) AIAA progress in aeronautics and astronautics, vol 90. AIAA, New York
37. Olivani A, Galfetti L, Severini F, Colombo G, Cozzi F, Lesma F, Sgobba M (2002) Aluminum particle size influence on ignition and combustion of AP/HTPB/Al solid rocket propellants, RTO-AVT Fall 2002 Meetings, Aalborg 23–27 Sept 2002
38. DeLuca LT, Galfetti L, Severini F, Meda L, Marra G, Vorozhtsov AB, Sedoi VB, Babuk VA (2005) Burning of *n*Al composite rocket propellants. Combust Explosion Shock Waves 41(6):680–692
39. DeLuca LT (2007) Burning of aluminized solid rocket propellants: from micrometric to nanometric fuel size. In: Ping H, Yajun W, Shengcai L (eds) Theory and practice of energetic materials, vol 7. Science Press, Beijing, pp 277–289
40. DeLuca LT, Galfetti L (2008) Burning of metallized composite solid rocket propellants: from micrometric to nanometric aluminum size, Asian joint conference on propulsion and power, Gyeongju, 6–8 March 2008
41. DeLuca LT, Galfetti L, Maggi F, Colombo G, Bandera A, Cerri S, Donegà P (2008) Burning of metallized composite solid rocket propellants: toward nanometric fuel size. In: Proceedings of ESA space propulsion, ESA, Crete, 05–08 May 2008
42. DeLuca LT, Bandera A, Maggi F (2009) Agglomeration of aluminized solid rocket propellants. AIAA paper 2009-5439, AIAA, Reston. doi:10.2514/6.2009-5439
43. DeLuca LT, Galfetti L, Colombo G, Maggi F, Bandera A, Babuk VA, Sinditskii VP (2010) Microstructure effects in aluminized solid rocket propellants. J Propuls Power 26(4): 724–733
44. Grigor'ev VG, Kutsenogii KP, Zarko VE (1981) Model of aluminum agglomeration during the combustion of a composite propellant. Combust Explosion Shock Waves 17(4):356–363
45. Cohen NS (1983) A pocket model for aluminum agglomeration in composite propellants. AIAA J 21(5):720–725
46. Babuk VA, Vasilyev VA, Malakhov MS (1999) Condensed combustion products at the burning surface of aluminized solid propellant. J Propuls Power 15(6):783–793
47. Babuk VA, Vasilyev VA, Sviridov VV (2000) Formation of condensed combustion products at the burning surface of solid rocket propellant. In: Yang V, Brill TB, Ren WZ (eds) Solid propellant chemistry, combustion, and motor interior ballistics, vol 185, AIAA Progress in Astronautics and Aeronautics. AIAA, Reston, pp 749–776
48. Babuk VA, Vasilyev VA, Glebov AA, Dolotkazin IN, Galeotta M, DeLuca LT (2004) Combustion mechanisms of AN-based aluminized solid rocket propellants. In: Novel energetic materials and applications, vol 9, IWCP. Grafiche GSS, Bergamo, paper 44
49. Babuk VA, Glebov A, Arkhipov VA, Vorozhtsov AB, Klyakin GF, Severini F, Galfetti L, DeLuca LT (2005) Dual-oxidizer solid rocket propellants for low-cost access to space. In: DeLuca LT, Sackheim RL, Palaszewski BA (eds) In-space propulsion, vol 10, IWCP. Grafiche GSS, Bergamo, paper 15
50. Babuk VA (2016) Chapter 13: Solid propellant formulation factors and properties of condensed combustion products. In: DeLuca LT, Shimada T, Sinditskii VP, Calabro M (eds) Chemical rocket propulsion: a comprehensive survey of energetic materials. Springer International Publishing, Cham

51. Rashkovskiy SA (1998) Metal agglomeration in solid propellants combustion—Part 2: Numerical experiments. Combust Explosion Shock Waves 136(1–6):149–169. doi:10.1080/00102209808924169
52. Gallier S (2009) A stochastic pocket model for aluminum agglomeration in solid propellants. Propellant Explos Pyrotechnics 34(2):97–105. doi:10.1002/prep.v34:2
53. Maggi F, DeLuca LT, Bandera A (2015) Pocket model for aluminum agglomeration based on propellant microstructure. AIAA Journal 53(11):3395–3403. doi:10.2514/1.J053992
54. Kraeutle KJ (1978) Particle size analysis in solid propellant combustion research. In: Boggs TL, Zinn BT (eds) Experimental diagnostics in combustion of solids, vol 63, AIAA Progress in astronautics and aeronautics. AIAA, New York, pp 76–108
55. Weiser V, Gettwert V, Franzin A, DeLuca LT et al (2016) Chapter 10: Combustion behavior of aluminum particles in ADN/GAP composite propellants. In: DeLuca LT, Shimada T, Sinditskii VP, Calabro M (eds) Chemical rocket propulsion: a comprehensive survey of energetic materials. Springer International Publishing, Cham
56. Dondé R, Guarnieri C, Meda L, Marra G, Orsini D, Prato A, Galfetti L, DeLuca LT (2007) Experimental investigations on transient burning of nano-aluminized solid rocket propellants, AAAF conference on changes in aeronautical and space systems, Avignon, 26–28 June 2006
57. Arkhipov VA, Bondarchuk SS, Korotkikh AG, Kuznetsov VT, Gromov AA, Volkov SA, Revyagin LN (2012) Influence of aluminum particle size on ignition and nonstationary combustion of heterogeneous condensed systems. Combust Explosion Shock Waves 48(5):625–635
58. Arkhipov VA, Korotkikh AG (2012) The influence of aluminum powder dispersity on composite solid propellants ignitability by laser radiation. Comb Flame 159(1):409–415
59. Zhao FQ, Yao EG, Xu SY, Li X, Xu HX, Hao HX (2016) Chapter 11: Laser ignition of different aluminum nanopowders for solid rocket propulsion. In: DeLuca LT, Shimada T, Sinditskii VP, Calabro M (eds) Chemical rocket propulsion: a comprehensive survey of energetic materials. Springer International Publishing, Cham
60. Arkhipov VA, Vorozhtsov AB, Shrager ER et al (2004) Acoustic admittance function study for solid propellants containing ultrafine aluminum. In: DeLuca LT, Galfetti L, Pesce-Rodriguez RA (eds) Novel energetic materials and applications. Proceedings of the IX international workshop on combustion and propulsion, Lerici, Italy, 14–18 Sept 2003. Grafiche GSS, Bergamo
61. Komarova M, Vorozhtsov AB (2014) Influence of passivated nanosized aluminum powder on physico-chemical characteristics of metalized compositions combustion. Russ Phys J 57(7):76–80
62. Lerner M, Glaskova E, Vorozhtsov AB, Rodkevich N et al (2015) Passivation of nanosized aluminum powder for use in high energetic materials. Russ J Phys Chem B (Khimicheskaya Foizika, in Russian) 9(1):56–61
63. Vorozhtsov AB, Zhukov A, Ziatdinov M, Bondarchuk S, Lerner M, Rodkevich N (2016) Chapter 9: Novel micro- and nanofuels: production, characterization, and applications for high energy materials. In: DeLuca LT, Shimada T, Sinditskii VP, Calabro M (eds) Chemical rocket propulsion: a comprehensive survey of energetic materials. Springer International Publishing, Cham
64. Sundaram DS, Yang V, Zarko VE (2015) Combustion of nano aluminum particles (review). Combust Explosion Shock Waves 51(2):173–196. © Pleiades Publishing, Ltd., 2015
65. Rosenband V, Gany A (2011) High-reactivity aluminum powders. J Energy Mater Chem Propuls 10(1):19–32
66. Yavor Y, Rosenband V, Gany A (2014) Reduced agglomeration in solid propellants containing porous aluminum. Proc Inst Mech Eng Part G 228(10):1857–1862
67. Hama A, Gany A, Palovuori K (2006) Combustion of activated aluminum. Combust Flame 145(3):464–480
68. Hama A (2010) Method of improving the burn rate and ignitability of aluminum fuel particles and aluminum fuel so modified. US Patent US 7785430 B2

69. Maggi F, Dossi S, Paravan C, DeLuca LT, Liljedahl M (2015) Activated aluminum powders for space propulsion. Powder Technol 270:46–52
70. Zhang DL (2004) Processing of advanced materials using high-energy mechanical milling. Prog Mater Sci 49(3–4):537–560
71. Koch CC, Whittenberger JD (1995) Review mechanical milling/alloying of intermetallics. Intermetallics 4(5):339–355
72. Filimonova VY, Korchagin MA, Evstigneev VV (2009) Anomalous decrease in the activation energy and initiation temperature of a thermal explosion in the mechanically activated composition 3Ni + Al. Dokl Phys 54(6):277–280
73. Shteinberg AS, Lin YC, Son SF, Mukasyan AS (2010) Kinetic of high temperature reaction in Ni-Al system: influence of mechanical activation. J Phys Chem A 114(20):6111–6116
74. Sippel TR, Son SF, Groven LJ (2013) Altering reactivity of aluminium with selective inclusion of polytetrafluoroethylene through mechanical activation. Propell Explos Pyrot 38(2):286–295
75. Dossi S (2014) Mechanically activated Al fuels for high performance solid rocket propellants. PhD Dissertation, Politecnico di Milano
76. Sippel TR, Son SF, Groven LJ et al (2014) Exploring mechanisms for agglomerate reduction in composite solid propellants with polyethylene inclusion modified aluminum. Combust Flame. (162): http://dx.doi.org/10.1016/j.combustflame.2014.08.013
77. Chan ML, Parr T, Hanson-Parr D, Bui T, Mason M (2004) Characterization of a boron containing propellant, In: DeLuca LT, Galfetti L, Pesce-Rodriguez RA (eds) Novel energetic materials and applications, IWCP vol 9, Paper 07. Grafiche GSS, Bergamo
78. Mitani T, Izumikawat M (1991) Combustion efficiencies of aluminum and boron in solid propellants. AIAA J Spacecr Rocket 28(1):79–84
79. Dossi S, Reina A, Maggi F, DeLuca LT (2012) Innovative metal fuels for solid rocket propulsion. Int J Energy Mater Chem Propuls 11(4):299–322
80. Shevchuk VG, Zolotko AN, Polishchuk DI (1975) Ignition of packed boron particles. Combust Explosion Shock Waves 11:189–192
81. DeLuca LT, Galfetti L, Maggi F, Colombo G, Reina A, Dossi S, Consonni D, Brambilla M (2012) Innovative metallized formulations for solid or hybrid rocket propulsion. Hanneng Cailiao/Chin J Energetic Mater 20(4):465–474. doi:10.3969/j.issn.1006-9941.2012.04.018. Presented at the *2011 IASPEP* (International Autumn Seminar on Propellants, Explosives and Pyrotechnics), China
82. DeLuca LT (2011) Energetic problems in aerospace propulsion. Politecnico di Milano, Milan
83. Fassina M (2015) Effects of Al particles shape on solid rocket propellant burning. PhD Dissertation, Politecnico di Milano, Milan, 16 February 2015
84. DeLuca LT, Galfetti L, Severini F, Rossettini L, Meda L, Marra G, D'Andrea B, Weiser V, Calabro M, Vorozhtsov AB, Glazunov AA, Pavlovets GJ (2007) Physical and ballistic characterization of AlH3-based space propellants. Aerosp Sci Technol 11:18–25
85. DeLuca LT, Rossettini L, Kappenstein Ch, Weiser V (2009) Ballistic characterization of AlH_3-based propellants for solid and hybrid rocket propulsion, AIAA Paper 2009–4874
86. Young G, Piekiel N, Chowdhury S, Zachariah MR (2010) Ignition behavior of α-AlH_3. Combust Sci Technol 182:1341–1359
87. Young G, Risha GA, Miller AG, Glass RA, Connell TL, Yetter RA (2010) Combustion of alane-based solid fuels. Int J Energetic Mater Chem Propuls 9(3):249–266
88. Young G, Jacob R, Zachariah MR (2015) High pressure ignition and combustion of aluminum hydride. Combust Sci Technol 187:1335–1350
89. Glorian J, Catoire L, Gallier S, Cesco N (2015) Gas-surface thermochemistry and kinetics for aluminum particle combustion. Proc Combust Inst 35:2439–2446
90. Komarov VF, Shandakov VA (1999) Solid fuels, their properties, and applications. Combust Explosion Shock Waves 35(2):139–143
91. Lipanov AM, Zarko VE (2016) Chapter 43: Survey of solid rocket propulsion in Russia. In: DeLuca LT, Shimada T, Sinditskii VP, Calabro M (eds) Chemical rocket propulsion: a comprehensive survey of energetic materials. Springer International Publishing, Cham